

Chapter 13

Dielectric Barrier Discharge (DBD) Plasmas and Their Applications

Deepak Prasad Subedi, Ujjwal Man Joshi and Chiow San Wong

13.1 Introduction

Gas discharge plasmas, also known as low-temperature plasmas, have drawn much attention in past few decades because of their importance in many technological developments. The use of plasma for industrial purposes began more than 100 years ago with the use of plasma sources for generation of ozone and also as light sources [1]. Since then, plasma processes have been utilized in a wide range of technological and research areas, including microelectronics, gas lasers, polymers treatments [2–4], synthesis of novel materials [5, 6], protective coatings [7–9], etc. Plasma processes are now commonly used in air cleaning systems, and treatment of food containers, fruits, meat, vegetables, fabrics, and medical devices [10]. New areas of application of plasma processes have also been established in recent years. This includes plasma nanotechnology that involves plasma-based production and modification of nanomaterials [11], plasma ignition, and plasma aerodynamics. Recent development in the production of atmospheric pressure plasma jet has extended the use of nonthermal plasma in biology and medicine for various applications such as dental treatment, wound healing, decontamination of surfaces, treatment of cancer cells, and other skin diseases [10, 12].

Among various sources of plasma, the dielectric barrier discharge (DBD) offers one of the most cost-effective nonthermal plasma sources. This type of discharge is known to be effective in the initiation of chemical and physical processes in gases [13]. DBD has been extensively studied in past few years because of its potential

D.P. Subedi (✉) · U.M. Joshi
Department of Natural Sciences, School of Science, Kathmandu University,
Dhulikhel, Nepal
e-mail: deepaksubedi2001@yahoo.com

C.S. Wong
Physics Department, Faculty of Science, Plasma Technology Research Centre,
University of Malaya, 50603 Kuala Lumpur, Malaysia

application in many different areas. It covers not only material processing but also applications in the field of energy and environment due to its ability to form highly reactive plasma at near room temperature with low energy consumption using simple reactor system at atmospheric pressure condition [14].

The first application of DBD plasma was in water treatment by ozone after Siemens proposed his novel idea to use DBD for ozone generation in 1857. It was reported in his paper that discharge initiated in an annular gap between two coaxial glass tubes could generate ozone from atmospheric pressure oxygen or air [1]. This invention led to the large-scale industrial production of ozone for the treatment of drinking water around 1900 in Europe. Novel application of DBDs in the production of flat panel television screens using AC plasma, reported in 1996, also drew much attraction [15]. The list of applications of DBD has been extended recently to at least two more fields of interest: airflow control and medicine [16].

The most important characteristic, which has made DBD profoundly useful in material processing, is its nonthermal equilibrium nature (refer Fig. 13.1). This nonthermal equilibrium plasma conditions can be established in DBDs in a much simpler way than with other alternatives such as low-pressure discharges, fast-pulsed high-pressure discharges, or by electron beam injection.

Figure 13.1 shows the dependence of electron temperature (T_e) and neutral temperature (T_g) on the pressure of mercury and rare gas mixture DBD plasma discharge. It is evident that there is a large difference between T_e ($\sim 10,000$ K) and T_g (~ 300 K) at a pressure of about 1 m Torr resulting in a nonthermal equilibrium plasma [17]. The difference in temperature between these two species arises due to low collision frequency between electron and neutral molecules at low pressure. However, at a pressure above 5 Torr, these two temperatures merge together to an average value of about 5000 K. The nonthermal equilibrium nature of these discharges has made them suitable for material processing.

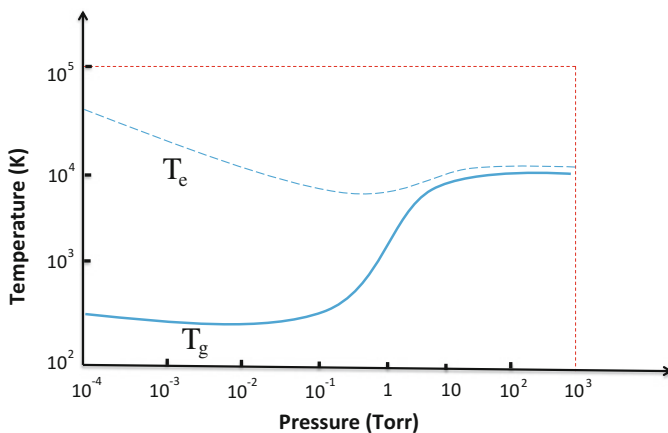


Fig. 13.1 Variation of electron and heavy particle temperature with pressure

13.2 Various Types of Plasmas Useful in Industry

There are various types of plasmas which are generated in research laboratories and many of them have been employed in industry. Classification of these wide range of plasmas can be made mainly on the basis of power supply used to generate them, pressure of the working gas, geometry of the electrode, and nature of the discharge. In the following sections, some low-pressure plasmas based on different power supplies will be discussed. This will be followed by a brief introduction to some plasmas which are generated in atmospheric pressure and are classified based on their discharge characteristics.

13.2.1 Low-Pressure Plasmas

There are many ways to generate a low-pressure plasma. The simplest and the oldest method is the DC glow discharge [18]. DC discharge is useful for sputter deposition of thin films of metals. It has a large potential drop at the conductive cathode producing an energetic bombardment of positive ions on cathode which sputter materials from the metallic cathode. However, they cannot be used to sputter dielectric materials or to deposit dielectric films since insulating surfaces become charged in opposition to the applied field. This problem is overcome using radio frequency (RF) or microwave (MW) discharges so that the positive charges accumulated during the one half cycle can be neutralized by electron bombardment during the next half cycle [19].

High-frequency (HF) plasma sources can be classified according to the type of external energy input used to sustain them. Plasma processing tools generally use RF and microwave power to sustain the plasma. Most commonly RF power is available at 13.56 MHz and microwave power is available at 2.45 GHz. Many types of HF plasma sources exist for processing applications and these are generally classified into capacitive, inductive, and types of EM wave sources used [20]. The latter two are also referred to as high density sources with electron density n_e 10^{17} m^{-3} . A brief review of low-pressure DC, RF, and microwave discharges will be presented in the following sections.

13.2.1.1 DC Discharge

DC glow discharge at low pressure is one of the most familiar of gaseous discharges because of the ease with which it can be generated and maintained and because of its distinctive appearance [21]. This is also one of the earliest forms of laboratory plasma originally studied by Faraday, Crookes, and others working on cathode ray

experiments. The appearance of the discharge is composed of several dark and luminous regions as shown in Fig. 13.2. The light emitted from luminous zones has specific colors which is the characteristic of the gas used. The discharge is produced by applying a DC voltage across two metal electrodes placed inside a glass tube evacuated and filled with a gas to a pressure in the range of 0.1–10 Torr. In a typical DC glow discharge, the voltage is of the order of few hundreds of volts, and the current is of the order of several milliamps [20]. The breakdown voltage V_B is a function of the pressure p of the gas inside the tube and the interelectrode distance d as expressed by Eq. 13.2.1 which is known as Paschen law.

$$V_B = f(pd) \quad (13.2.1)$$

The voltage (V) along the discharge is found experimentally to vary as shown in the lower part of Fig. 13.2. The associated curve for the axial electric field (E) can readily be found from the voltage distribution. If the distance between the two electrodes is reduced keeping the pressure constant, it is found that the reduction in length is taken up entirely by the positive column of the discharge. The positive column constitutes a plasma which is an ionized gas with no net space charge. A detailed description of the different dark and luminous regions in the discharge tube can be found in earlier work [21].

In fact, most of the modern plasma devices are the modified version of the low-pressure glow discharge tube. In practical applications of the discharge for material processing, the electrode area is enlarged whereas the interelectrode distance is reduced. When the distance between the electrodes is made much smaller compared to the dimension of the electrode, most of the discharge will be occupied by the positive column providing a bulk of stable and homogeneous plasma.

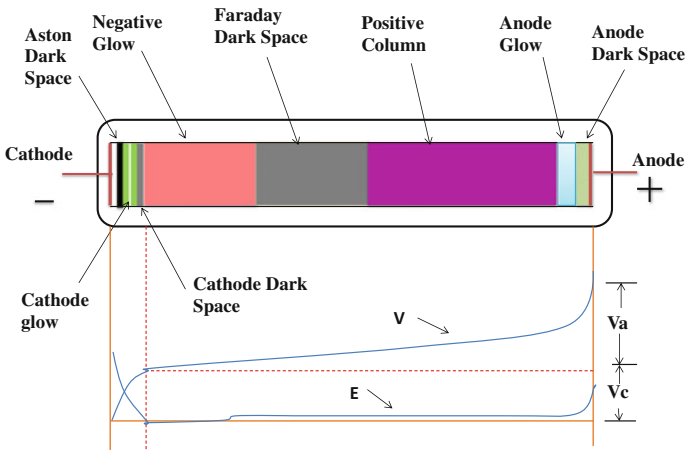


Fig. 13.2 Schematic diagram of the luminous zones and dark spaces in a low-pressure DC glow discharge

13.2.1.2 RF Discharge

When an alternating electric field is applied to a gas, the DC breakdown characteristics are still applicable if the frequency is below about 1 kHz. In this low frequency range, the time for one cycle of the applied AC field is much longer than the ion transit time in the plasma. However, for higher frequencies, AC breakdown takes place at peak voltages differing from the corresponding DC values [21]. At frequencies of the order of 100 kHz, the breakdown voltage is not only a function of (pd) as in the case of DC discharge but also depends on (fd) as represented by the following equation:

$$V_B = f'(pd, fd), \quad (13.2.2)$$

where f is frequency of the RF source. Radio frequency discharge is one of the most widely used discharge types in application for thin film deposition because of its ability to generate a large volume of stable and homogenous plasma. The commercially available RF power supplies are operated at a frequency of 13.56 MHz. Based on the method of coupling, the high-frequency power with the load, the high-frequency discharges are usually classified into two types: (i) capacitive coupling and (ii) inductive coupling.

The capacitively coupled internal electrode type which is also referred as parallel-plate or diode RF system has been widely used as production-level plasma reactors. The main reason for their wide application is due to its ease of scale-up [22]. The schematic drawing of a typical capacitively coupled RF plasma reactor is shown in Fig. 13.3.

A plasma is formed in the space between the electrodes due to the applied electric field. The region between the plasma and both the electrodes and the walls

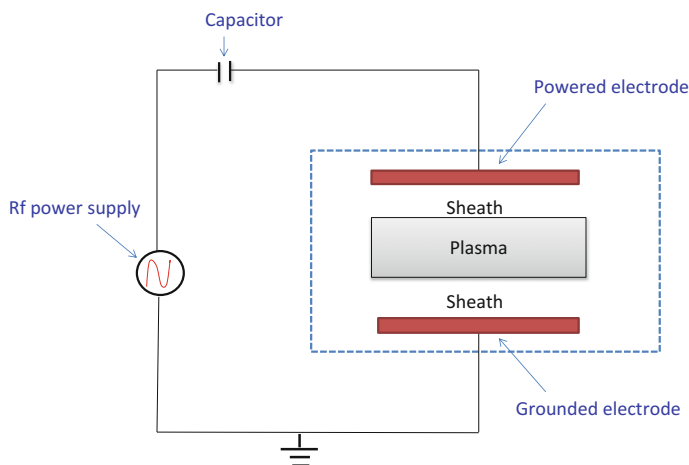


Fig. 13.3 Schematic diagram of AC-coupled RF plasma reactor

of the reactor is known as the sheath. The sheath plays an important role in the use of plasma for various applications because it is the region where the charged particles gain kinetic energy to bombard the surfaces to be treated by plasma. The reactors are said to be capacitively coupled because the radio frequency currents and voltages that sustain the plasma are introduced through the sheath, which acts like a capacitive element in an electrical circuit [23]. These sources employ one or more electrodes to produce plasma, with typical electrode voltages of 100–1000 V and typical RF powers of 100–1000 W. Low-pressure RF discharges are widely used for deposition of thin films by plasma-enhanced chemical vapor deposition (PECVD). Zajickova et al. [8] used PECVD based on hexamethyldisiloxane (HMDSO) monomers to deposit SiO₂ protective films on polycarbonate (PC). Dependence of the sputtering of PC on the applied RF power and the self-bias voltage in argon plasma was also investigated in this study. It was found that the sputtering rate is proportional to these two discharge parameters.

A more detailed investigation on the surface treatment of polycarbonate substrate by low-pressure RF discharge and its effect on film deposition can also be found in an earlier work by Zajickova et al. [9]. This study revealed that treatment of the substrate in argon discharge prior to the deposition of the thin film considerably increased the adhesion of the film to the substrate.

At low pressures, a stable glow discharge can be easily generated, whereas it is difficult to get a stable homogeneous glow discharge at atmospheric pressure. Recently, RF power sources are also used to generate stable glow discharge in atmospheric pressure plasma using DBD configuration. Moon et al. [24] performed a feasibility study of controlling plasma at atmospheric pressure by investigating the role of helium gas in an argon glow plasma using 13.56 MHz radio frequency power. This study suggests that mixing of the supply gas is a useful way of controlling the plasma characteristics that may be utilized for applications with specific required discharge conditions.

13.2.1.3 Microwave Discharge

Microwave discharges are widely used for generation of quasi-equilibrium and nonequilibrium plasma for different applications. Microwave plasma can be generated at pressures from 10⁻⁵ Torr up to atmospheric pressure in the pulse and continuous wave regimes at incident powers ranging between several watts and hundreds of kW [25].

At this range of frequency of the power supply, ions and subsequently the electrons also can no longer reach the electrodes as they are unable to follow the rapidly oscillating field. No secondary electron emission is required to sustain the discharge. This makes it possible to have electrode less discharge. Therefore, the power can be concentrated to a localized volume and thus a high-density plasma can be generated [20]. The density of ions in such a plasma can be more than $3 \times 10^{11} \text{ cm}^{-3}$. The most commonly used frequency of the microwave power

supply is 2.45 GHz corresponding to a wavelength of 12.24 cm which is roughly comparable to the dimension of a typical microwave reactor [26].

In 2012, Hoskinson et al. [27] demonstrated a novel array of micro-plasma sources consisting of microwave resonators arranged in a two-dimensional grid. This study verified the electromagnetic behavior of the array through application of analytic coupled mode theory, electromagnetic modeling, and observation of the generated plasma structures. Their investigations showed that the device in specific mode could be useful for applications in material and surface modifications. Microwave resonator-based discharges offer several advantages compared to DC or low-frequency micro-plasma discharges.

A topical review on the methods of microwave plasma generation, general features of microwave plasma, and selected aspects of microwave plasma diagnostics can be found in an earlier work [25].

13.2.2 Atmospheric Pressure Plasma

Atmospheric pressure nonequilibrium plasmas have made a remarkable progress in plasma generation techniques recently, including atmospheric pressure glow discharge (APGD) [28–32], dielectric barrier discharge (DBD) [1], corona discharge [33, 34], surface discharge [35–37], pulsed discharge [14, 38, 39], etc. This has led to an expansion of their applications into the field of energy and environment as well as material conversion processes [14]. The widespread application of these discharges is driven mainly by virtue of their special advantage of forming a highly reactive plasma at near room temperature condition with low energy consumption using simple reactor system at atmospheric pressure.

An extended review of atmospheric pressure discharges producing nonthermal plasma has been presented in a paper by Navartovich [15] which reports the classification of such discharges with respect to their properties, and an overview of their possible applications. Several research papers have been published reporting new developments in the form and applications of atmospheric pressure plasmas in past one and a half decade.

In the following sections, corona discharge, arc discharge, surface barrier discharge (SBD), dielectric barrier discharge (DBD), and atmospheric pressure glow discharge (APGD) are briefly reviewed with some recent developments and their new areas of applications.

13.2.2.1 Corona Discharge

Generally, a corona discharge is obtained when the discharge current is limited to the micro-ampere level after electrical breakdown has been achieved. A specific form of corona discharge at atmospheric pressure is the luminous glow localized in space around a point tip in a highly nonuniform electric field [17]. Figure 13.4

shows the schematic diagram of a typical point-to-plane corona discharge. In this type of discharge, the geometry of the electrode confines the gas ionizing process to high-field ionization region around the active pointed electrode. Usually, the corona geometry is named positive, negative, bipolar, AC, or high frequency (HF), according to the polarity of the active electrode. The space between the active pointed electrode and the plane electrode can be divided into two regions: (i) the ionization region and (ii) the drift region. The ionization region is concentrated very close to the pointed electrode. The region outside this is the drift region where ions and electrons react with the neutrals but with too low energy to ionize and too low density to react with other ionized particles [33]. The application of corona discharge in processing of materials is limited due to the restricted area of the discharge. However, several attempts have been made to overcome this limitation using two-dimensional arrays of electrodes. Main applications of corona discharge are in the fields of surface modification of polymers, ozone generation, particle precipitation, and enhancement of SiO_2 growth during thermal oxidation of silicon wafers [17]. Schutze et al. reported that for a positive point-to-plane corona discharge operating in air at 760 Torr, the plasma was ignited at 2–5 kV and produced extremely small current of the order of 10^{-10} – 10^{-5} A.

Akishev et al. [34] investigated the phenomenology of a high-current negative point-to-plane corona in nitrogen. They found that the structure and current–voltage characteristic of the corona change significantly when the working gas is slowly blown through the discharge cell. They also studied the time evolution of the radial profile of the current density at the anode under different experimental conditions.

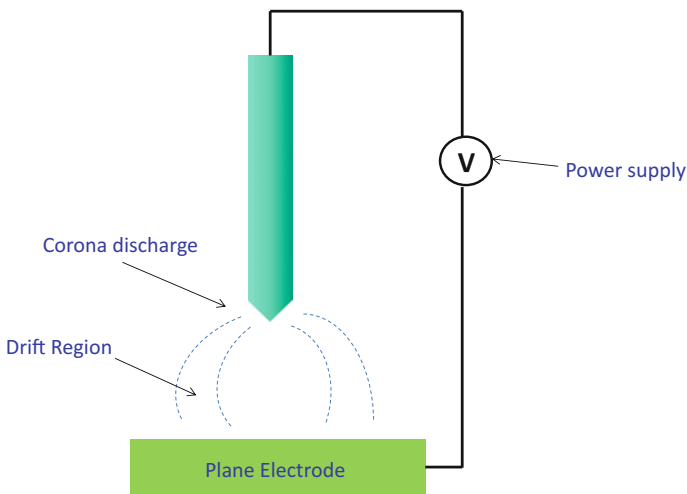


Fig. 13.4 Schematic diagram of a point-to-plane corona discharge

13.2.2.2 Arc Discharge

An arc discharge is obtained when the discharge current is maintained at above ampere level after an electrical breakdown of a gas has occurred. A thermal arc discharge will be produced when the filling gas pressure is sufficiently high.

Figure 13.5 shows the current–voltage characteristics of a gas discharge showing the Townsend (Dark) discharge, corona discharge, glow discharge, and arc discharge regions. It is evident from the figure that an arc discharge can be maintained by a lower voltage than a glow discharge. Further details on current–voltage characteristics of gas discharge can be found in an open source [40].

Arc discharges are commonly used in metallurgical processes, e.g., to melt rocks containing Al_2O_3 to produce aluminum and synthesis of carbon nanoparticles [41]. Fanara et al. [42] made a detailed investigation on the properties of atmospheric pressure arc by means of electric exploration of the plasma column and the anode region. A multi-wire apparatus, operating for arc currents in the range 50–200 A has been described and the ion current density and temperature maps are also shown in their study.

In order to obtain a nonthermal plasma at atmospheric pressure discharge, the first step is to avoid the formation of an arc. This can be achieved by limiting the current flowing through the discharge. Use of dielectric barrier between the electrodes can be made to limit the current in the discharge thereby converting it into high-voltage, low-current discharge. This type of discharge system in which either one or both of the electrodes are covered by dielectric barrier is called a dielectric barrier discharge (DBD).

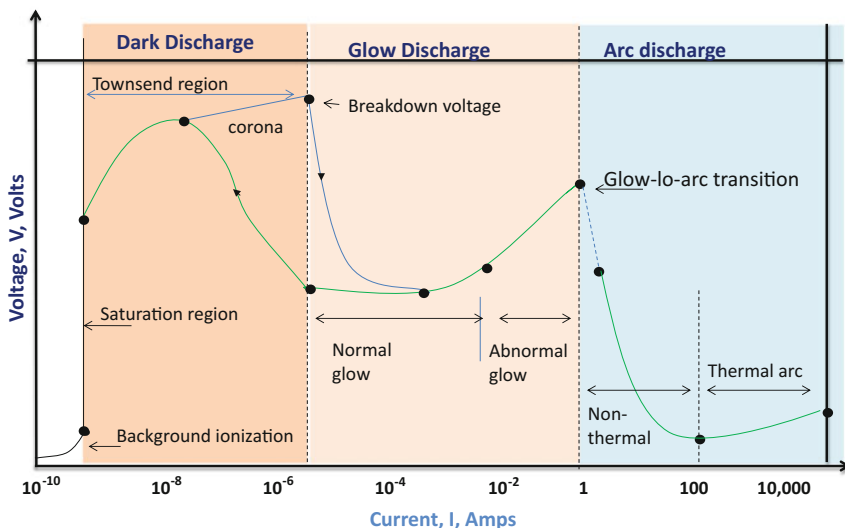


Fig. 13.5 Current voltage characteristics of gas discharge showing the Townsend (Dark) discharge, corona discharge, and arc discharge regions

13.2.2.3 Dielectric Barrier Discharge (DBD)

In the study of gaseous discharge, there are two main ways to prevent the transition of a discharge from corona to spark. One approach is to use a nanosecond pulse power supply [43]. The other approach is to insert a dielectric barrier in the discharge gap. The insertion of dielectric material in the discharge gap is to limit the discharge current thereby preventing the formation of complete breakdown. The schematic diagram of a DBD system is shown in Fig. 13.6. Due to the absence of complete breakdown, DBD is sometimes called silent discharge.

The dielectric barrier discharge (DBD) has a number of possible industrial applications and has been a subject of research for many years [44]. It possesses potential advantages in atmospheric pressure surface processing and plasma chemistry. The most important characteristic of DBD is that a nonthermal equilibrium plasma condition can be achieved in a much simpler way compared to other alternatives like low-pressure discharges, fast-pulsed high-pressure discharges, or electron beam injection. The flexibility with respect to geometrical configuration, operating medium, and operating parameters is another important advantage of atmospheric pressure DBD.

Moreover, the conditions optimized in laboratory experiments can easily be scaled up to large industrial installations [45]. In 2004, Laroussi and Lu [38] presented a study on the power consideration in the pulsed dielectric barrier discharge at atmospheric pressure. Pulsed operation with pulse widths in the range of nanoseconds has been suggested to enhance the plasma chemical processes. This study reports on a specially designed, dielectric barrier discharge-based diffuse-pulsed discharge and its electrical characteristics. Their results indicated that the mechanism in this system would lead to a much improved power transfer to the plasma.

In a recent study by Gibalov and Pietsch [16], dynamics of dielectric barrier discharges in different arrangements has been investigated. Based on experimental results, they have performed numerical investigations of DBDs in three basic configurations: volume, coplanar, and surface discharge arrangements. This study found that the anode- and cathode-directed streamers appear with a highly

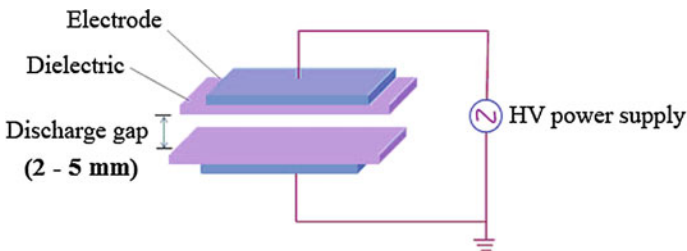


Fig. 13.6 Schematic diagram of a parallel-plate DBD

conductive channel in between. The interaction of the streamers with conductive and dielectric surfaces determines the filamentary or homogeneous appearance of the discharge and its properties.

13.2.2.4 Surface Barrier Discharge (SBD)

There are several terms used in literature to describe surface discharge. They are often named as sliding discharge and/or creeping discharge. A surface discharge is called dielectric barrier discharge (DBD) when one or both the electrodes are covered by dielectric material. SBDs are commonly used for surface treatment of materials, ozone generation, aerodynamics, etc. Schematics of typical surface barrier discharge systems are shown in Fig. 13.7.

A detailed investigation of SBD generation and its application for surface modification of polypropylene nonwoven fabrics has been reported in an earlier work by Cernakova et al. [35]. An experimental study of a SBD for the active control of subsonic airflow has been made by Dong et al. [36]. This study also performed complementary and coherent electrical, optical, and aerodynamic measurements as a function of various parameters and geometries. They have investigated the influence of the frequency and applied voltage of the discharge on the dissipated power. Their investigation resulted in an empirical formula to calculate the dissipated power and the energy lost in the dielectric.

In 2009, Cech et al. [46] reported on the influence of electrode gap width on plasma properties of diffuse coplanar surface barrier discharge in nitrogen. They studied the plasma parameters by means of time- and space-resolved optical emission spectroscopy and oscilloscopic measurements which provided a spatial and temporal distribution of the luminosity of the discharge. An elaborated description on SBD can also be found in an earlier report [37].

13.2.2.5 Atmospheric Pressure Glow Discharge (APGD)

The APGDs are closely related to DBDs and they are operated in a similar discharge configuration with high-voltage electrodes that are covered by dielectric barriers that lead to self-quenching of the micro-discharges and prevention of spark formation [47].

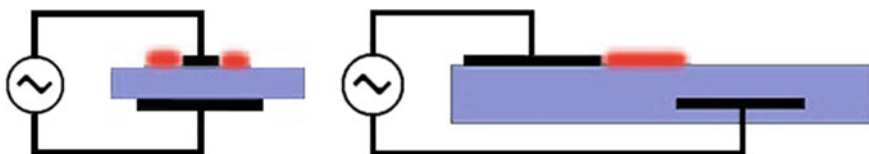


Fig. 13.7 Examples of surface DBD configurations. Reprinted from Kogelschatz [37] with permission

The DBD at atmospheric pressure usually has a filamentary nonhomogeneous form. The first step to get a homogeneous discharge at atmospheric pressure consists of avoiding the formation of a streamer and then of a micro-discharge. The origin of the streamer is a large electronic avalanche creating enough ions to localize the electrical field. The streamer formation is observed when the gas gap becomes large compared with the electron mean free path. At room temperature, the transition between the Townsend and the streamer breakdown occurs when the product of the gas gap and the pressure (pd) becomes around 100 Torr cm. An easy solution to avoid streamer formation at atmospheric pressure has been suggested by Massines et al. The solution consists of using micro-plasmas made in micrometric cells. Another solution consists of heating the gas in order to decrease its density [48]. Several researchers have tried to obtain the homogeneous DBD at atmospheric pressure [49, 50]. Okazaki et al. [50] were able to show that a uniform DBD could be generated under specific condition of power supply and electrode configuration. They named such discharge as APGD. Their study showed that DBD can be made homogeneous, if the frequency of the power supply is higher than 1 kHz and if helium or argon with a small admixture of acetone is used. A new technique of stabilizing the homogeneous glow discharge at atmospheric pressure by 50 Hz source in any gas was reported by Okazaki et al. [50]. Due to the possibility of using line frequency power supply, this system could be more cost-effective compared to the systems which work with power supplies of frequencies in the range of kHz or MHz.

In 2001, Trunec et al. [49] reported the generation of atmospheric pressure glow discharge in neon. They investigated the electrical characteristics of APGD in neon for different voltages and frequencies of power supply and different gas flows. This study also made a comparison of electrical properties of the discharges in neon with that of the discharge in argon and in the mixture of neon with argon.

Chen et al. [30] presented a preliminary discharging characterization of a novel APGD plume and its application in organic contaminant degradation. They were able to generate an atmospheric pressure glow discharge plume (APGD-p) using a dielectric barrier discharge reactor with one conductive liquid electrode. Their results showed that the APGD reactor produced a cold plasma plume with temperature not higher than 320 K at power of 5–50 W.

In another work reported in 2007, Buntat et al. [31] reported the generation of a homogeneous glow discharge in air at atmospheric pressure. They have experimentally investigated the discharge using two different electrode configurations of a perforated aluminum sheet and stainless steel wire mesh. This study showed that the perforated material shows a better glow discharge stabilization than that of stainless steel wire mesh.

13.3 Generation and Characterization of DBD

13.3.1 Introduction

DBD systems can be made in many configurations. The most convenient is the planar-type DBD using parallel plates separated by a dielectric material. Cylindrical DBDs are also widely used for ozone generation. This system is made using coaxial tubes with a dielectric material between them. The schematics of planar and cylindrical DBDs are shown in Fig. 13.8 [1]. This discharge requires alternating voltage for operation due to the presence of a dielectric barrier between electrodes. The interelectrode distance may considerably depend upon the type of DBD. In plasma displays, it is less than 0.1 mm where as it can be up to several millimeters in ozone generators and up to several centimeters in the case of CO₂ lasers. In the DBD systems described here, the interelectrode distance is varied from 1 to 3 mm.

13.3.2 Principle and Operation of DBD

As a consequence of the presence of at least one dielectric barrier, the DBD acts as a capacitor. Its capacitance is contributed by both the dielectric and the air/gas space. The capacitance, in combination with the time derivative of the applied

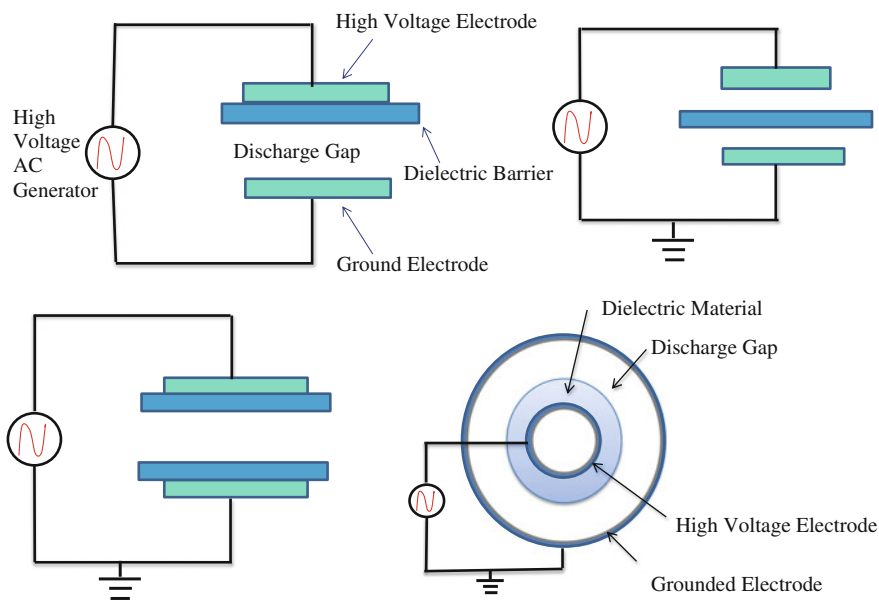


Fig. 13.8 Common dielectric barrier discharge configurations

voltage determine the amount of displacement current that can be passed through the DBD. The main discharge current flows through the DBD when the electric field is high enough to cause breakdown in the discharge gap. In most applications, the dielectric limits the average current density in the gas space. It thus acts as a ballast which, in ideal case, does not consume energy. Preferred materials for the dielectric barrier are glass, quartz, ceramics, thin enamel, or polymer layers or other materials of low dielectric loss and high breakdown strength. In some applications, additional protective or functional coatings are applied. At very high frequencies, the current limitation by the dielectric becomes less effective. For this reason, DBDs are normally operated between line frequency and 10 MHz. When the electric field in the discharge gap is high enough to cause the breakdown, in most gases a large number of micro-discharges are observed when the pressure is of the order of 10^5 Pa (atmospheric pressure). This is a preferred pressure range for ozone generation, pollution control as well as material processing and polymer surface modification.

To generate a discharge, one of the electrodes is connected to the high-voltage power supply with voltages in the range of a few hundred volts to several hundred kilovolts (operated between line frequency and about 10 MHz as mentioned above) through a ballast resistor (5–20 M Ω) in series to limit the current which prevents the electric puncture in case of material processing and polymer surface modification. Another electrode is grounded through a shunt resistor of 10 k Ω across which the discharge current is measured. The voltage applied to the electrodes can be measured by a high-voltage probe. In case of atmospheric pressure DBD, the most common electrical diagnostic consists of the measurement of the voltage applied to the electrodes and the discharge current. The voltage across the shunt resistor connected in series to ground yields the discharge current. The current and voltage waveforms can be recorded with the help of a digital oscilloscope. From these observations, current–voltage characteristics and breakdown characteristics can be obtained. The characteristics of the breakdown and the formation of the discharge are sensitive to the electrode gap, applied voltage, and ballast resistor which affect the uniformity in its applications such as material processing, polymer surface modification, etc. For optical characterization, the optical emission spectroscopy (OES) method is commonly used.

When the electric field in the discharge gap is high enough to cause breakdown, in most gases a large number of micro-discharges are observed when the pressure is of the order of 10^5 Pa (atmospheric pressure). Figure 13.9 (left) shows the micro-discharges in a 1-mm gap containing atmospheric pressure air, photographed through a transparent electrode. In this filamentary mode, plasma formations resulting in electrical conductivity are restricted to the micro-discharges. The gas in between is not ionized and serves as a background reservoir to absorb the energy dissipated in the micro-discharges and to collect and transport the long-lived species created.

The dielectric is the key for the proper functioning of the discharge. Once ionization occurs at a location in the discharge gap, the transported charges accumulate on the dielectric. The field due to the accumulated charges reduces the field

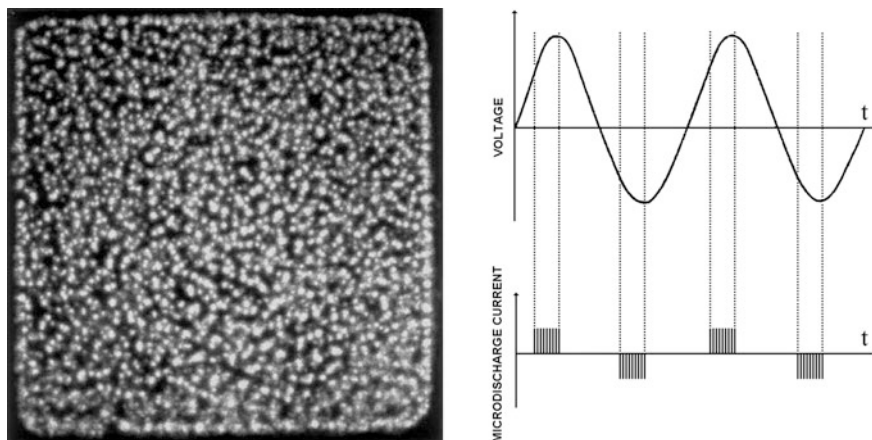


Fig. 13.9 End-on view of micro-discharges (*left*) and schematic diagram of bursts of micro-discharges (*right*) (Eliason 1997)

in the gap and interrupts the current flow after a few nanoseconds. The duration of the current pulse depends on the pressure and the effective ionization characteristics of the gas as well as on the dielectric properties. By applying a sinusoidal voltage of sufficient amplitude, a large number of such micro-discharges of nanosecond duration are formed. They are randomly distributed in space and time. The DBD produced at atmospheric pressure usually has nonhomogeneous filamentary nature. At the maximum and minimum of the applied voltage, the displacement current is zero and the micro-discharge activity stops, only to start again when the breakdown field is reached in the gap during the next half cycle (Fig. 13.9). The dielectric serves two functions: it limits the amount of charge transported by a single micro-discharge, and ensures that the micro-discharges present are distributed over the entire electrode area.

13.3.3 Generation of DBD Plasma in Different Configurations

The geometry of electrodes plays significant role in determining the value of potential and the electric field strength between the interelectrode spacing where the DBD plasma is formed. The interelectrode distance and thickness of dielectric barrier have equally important role in the production of DBD plasma. DBDs generated using different types of electrodes are briefly described in the following sections.

13.3.3.1 Parallel-Plate Electrode System

The schematic diagram of a parallel-plate DBD system is shown in Fig. 13.10. The discharge is generated between two symmetric electrodes. The electrodes are made of brass with smooth surface. They have 50 mm diameter and 10 mm thickness. The lower electrode is fixed and the upper one is movable with a pitch of 0.5 mm. Glass plate of 2 mm thickness is used as the dielectric barrier. A high-voltage AC power supply is used and the applied voltage is in the range of 1–2 kV at a frequency of 30 kHz. The gap between the electrodes can be varied from 0.5 to 2 mm and Ar is fed at a flow rate of 1 l/min. The experiments are carried out for gap spacing of 0.5, 1–2 mm.

This system was studied by electrical and optical measurements. Electron temperature and electron density in the discharge were measured by power balance method and line intensity ratio method. Effect of this plasma treatment on the surface property of polymers was also investigated by contact angle measurement. Contact angle measurement on untreated and plasma-treated samples showed that this discharge effectively improves the wettability of the polymer surface [51].

13.3.3.2 Cylindrical Electrode System

The schematic of a typical DBD system with cylindrical electrodes is shown in Fig. 13.11a. Two electrodes are held parallel to each other horizontally in stand. The electrode consists of glass tube filled with fine brass powder with a central wire inside. The internal diameter of the tube is 12.6 mm and external diameter is 14.9 mm with 1.2 mm thick glass as dielectric barrier. The electrodes are 126.2 mm in length. They are separated by 2.9 mm distance where DBD is produced. The fine metallic powder packed inside the glass tube serves as electrode to produce electric discharge. The photograph of the discharge is depicted in Fig. 13.11b.

The electrodes used in this system are designed for an easy passage of long rolls of textiles and other materials for continuous treatment in plasma. As an example, a

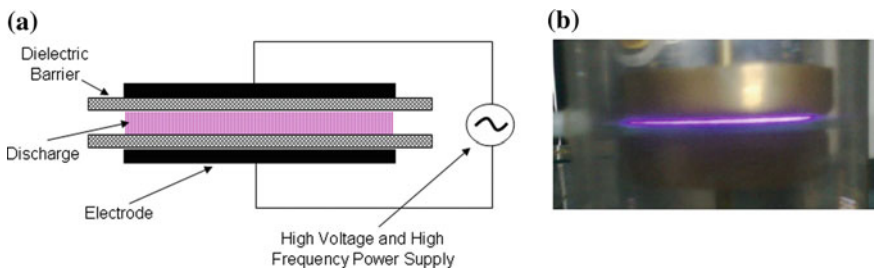


Fig. 13.10 Schematic diagram DBD with parallel-plate electrodes with double barrier (a) and photograph of the discharge (b) [51]

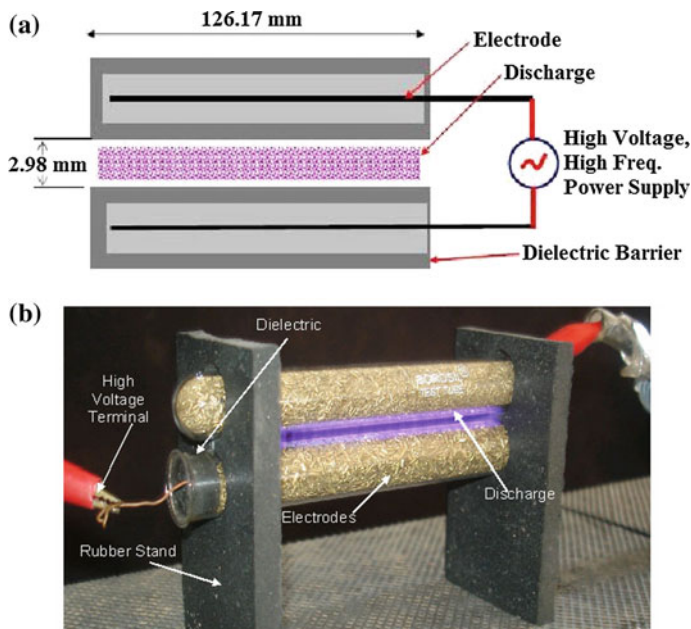


Fig. 13.11 **a** Schematic diagram of DBD with cylindrical electrodes. **b** Photograph of the discharge

cotton fabric driven by an electric motor was passed through the discharge between the electrodes and the improvement in wettability of the sample was investigated by contact angle measurement. Figure 13.12 shows the image of water drops on the untreated and plasma-treated samples. It was observed that the cotton sample which was hydrophobic before treatment turned into hydrophilic after 20 cycles of treatment through the discharge.

13.3.3.3 Coaxial Electrode System

DBD with coaxial cylindrical electrode system is mainly used for chemical syntheses such as generation of ozone and treatment of engine exhaust gas. It is designed to provide an annular gap between two coaxial tubes and a radial electric field is applied by a high-voltage AC power supply. It causes an electrical breakdown of the flowing gas in the annular gap. Early experiments conducted in such a system showed that some oxygen molecules in the air flowing through the discharge gap between the glass tubes are converted to ozone. In the present experiment, a HV power supply of amplitude 18 kV operating at line frequency of 50 Hz is applied across the two cylindrical electrodes. The central electrode is made of brass rod (diameter is 3 mm, length 65 mm) and enclosed by an inner cylindrical glass tube. The outer electrode is made of aluminum foil which wraps around the

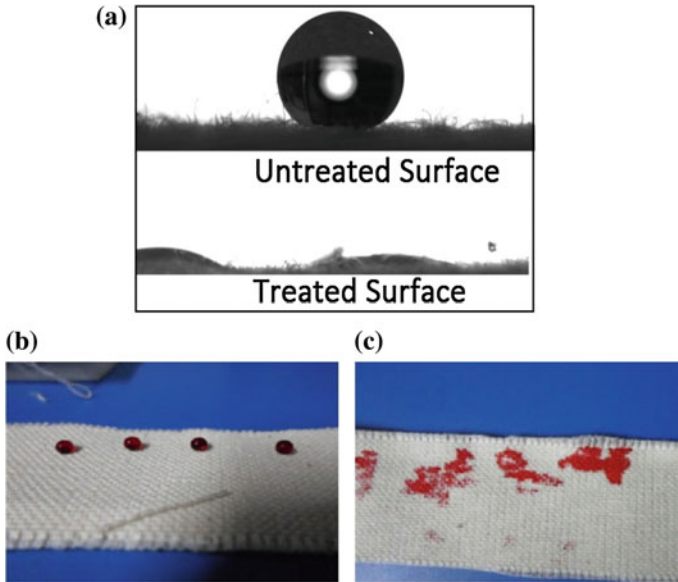


Fig. 13.12 Images of water drops on untreated and plasma-treated surface of cotton fabric (a, b). A complete wetting was obtained after 20 cycles of treatment (c) Image reproduced from the permission of authors: doi:10.1063/1.4993084

outer cylindrical glass tube. The gap between the two dielectric layers is 3 mm through which air or water can easily flow. In our experiments, we used the system for direct treatment of water by electric discharge. Figure 13.13 shows the cross-sectional view of the coaxial electrode system in a DBD. The main objective of the work was to develop a system in which water could be passed through the annular gap between the electrodes making the treatment more effective. Water from different sources such as river, well, stone spout, and tap was treated by this method. The general evaluation of the efficiency of the treatment for water disinfection was made. The experimental results show that the qualities of water such as pH, conductivity, chlorides, and total hardness of water changed slightly after treatment. However, the coliforms and chemical oxygen demand (COD) were significantly reduced in the treated samples. A remarkable increase in the amount of dissolved oxygen (DO) was also observed after the treatment [52].

13.3.3.4 Atmospheric Pressure Plasma Jet (APPJ)

In the previous sections, we mentioned that the atmospheric pressure plasma can be generated in various configurations. The main problem with these systems is that the working space is often limited because of the small gap between the electrodes.

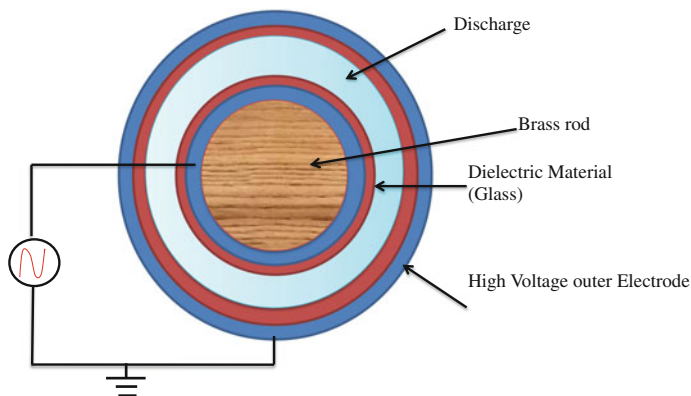


Fig. 13.13 Cross-sectional view of the coaxial electrode system in a DBD

In an atmospheric pressure plasma jet, the plasma constituents are expelled through an orifice by a gas flow which makes the treatment of large objects possible. Forster et al. [53] reported an atmospheric pressure plasma jet in a DBD configuration. This type of discharge can be operated under high gas flow rate. In 2003, Toshifuji et al. [54] reported a relatively cold arc plasma jet produced under atmospheric pressure having potential application for surface modification. Recently, Takemura et al. [55] developed an APPJ with long flame which can be used to modify polymer film with a work distance of over 200 mm. Similarly, a double-layered APPJ had also been reported in 2009 [56]. It consists of an additional part in the jet system for introduction of nitrogen gas into the outer nozzle between the inner and outer tubes boosting the plasma plume which results in a brighter and longer plasma torch. This system is supposed to have more radicals which may broaden the application range of atmospheric pressure plasma jets. Kuwabara et al. have presented a detailed investigation on the effects of electrode positioning on the atmospheric pressure plasma torch based on DBD configuration [57]. In this work, the authors also discussed the factors which determine the length of plasma jet.

In our study, a nonthermal nitrogen plasma jet was generated using a high-voltage power supply with output frequency of 10–30 kHz under atmospheric pressure. The experimental setup used to generate atmospheric pressure plasma jet is shown in Fig. 13.14. The dependence of the length of plasma jet on the gas flow rate was investigated and application of this plasma jet to the surface modification of polymer material was also demonstrated.

Figure 13.15 shows that the length of plasma jet can be enhanced up to 75 mm by increasing the gas flow rate from 1 to 4 l/min. However, there was no further change in length beyond this flow rate.

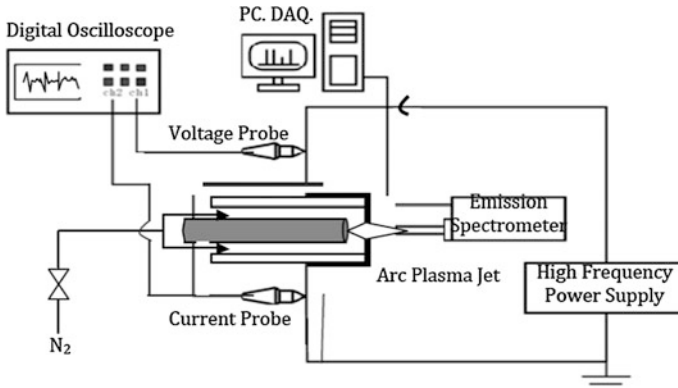


Fig. 13.14 Schematic diagram of atmospheric pressure plasma jet system. Reproduced from Subedi et al. [58] with permission from the editor

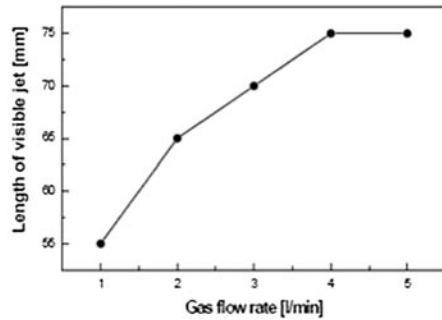
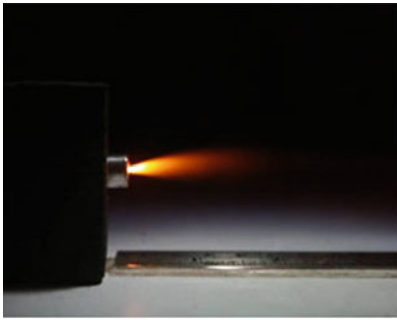


Fig. 13.15 Photograph of plasma jet and the dependence of jet length on gas flow rate. Reproduced from Subedi et al. [58] with permission from the editor

13.3.4 Characterization of DBD

Different methods are available to measure the electron density and electron temperature in a plasma. The most commonly used methods are: Langmuir probe, microwave interferometer, Laser Thomson Scattering [LTS], optical emission, and absorption spectroscopy [59].

Characterization of the discharge by analyzing the emission spectra is a powerful tool for the diagnostic of plasma.

To determine the electron temperature (T_e) and electron density (n_e) in low-pressure plasma, probe method is widely used but the application of probe method to atmospheric pressure plasma is difficult due to small discharge gap distance [60]. Alternatively, a powerful tool widely used for the plasma diagnostic is optical emission spectroscopy (OES), which is nonintrusive and gives rich

information about the plasma species. By analyzing and interpreting the plasma spectra, we can obtain the important properties of the plasma, such as temperature, density of chemical species, and ionization state [61].

13.3.4.1 Electrical Characterization

In DBD, electric current (i) flows between the electrodes through a defined plasma volume with cross section A and there is no current loss to the surrounding. This makes it possible to use the measured current as a diagnostic tool for plasma generated at atmospheric pressure. The current density (j) is a function of electron density (n_e) and drift velocity (v_d) of electrons according to Eq. 13.3.1 which in turn is a function of electric field.

$$j = n_e e v_d \quad (13.3.1)$$

In order to determine n_e from Eq. 13.3.1, values of v_d for different electric field values can be found from literature. Alternatively, it is also possible to use the measured values of applied voltage and average discharge current to estimate the electron density n_e . This method is termed as power balance method and is described by the following equation:

$$n_e = \frac{P_{av}}{2Av_b E_{lost}}, \quad (13.3.2)$$

where P_{av} is the average power, A is the area of the electrode, v_b is Bohm velocity, and E_{lost} is the energy lost by the system per electron-ion pair. In a recent study, Eq. 13.3.2 was used to estimate the electron density in argon discharge produced in parallel-plate DBD [62]. A high-voltage probe was used to measure the voltage applied across the electrodes while the discharge current was measured using a shunt resistor at the earth side of the discharge tube.

The signals were recorded using a Tektronix TDS2002 digital oscilloscope. Figure 13.16 shows the applied voltage and discharge current waveforms obtained in an argon discharge.

Taking Bohm velocity $v_b = 2 \times 10^3$ m/s and energy lost $E_{lost} = 50$ eV; and using the values of electrode area $A = 17.5 \times 10^{-4}$ m², applied voltage $V_{rms} = 13$ kV, and average discharge current $I_{rms} = 3.86 \times 10^{-5}$ A from the current waveform shown in Fig. 13.16 and substituting in Eq. (13.3.2), the electron density in air plasma was found to be equal to $n_e = 8.97 \times 10^{11}$ cm⁻³ which is in fairly good agreement with the values of electron density in low-temperature plasmas.

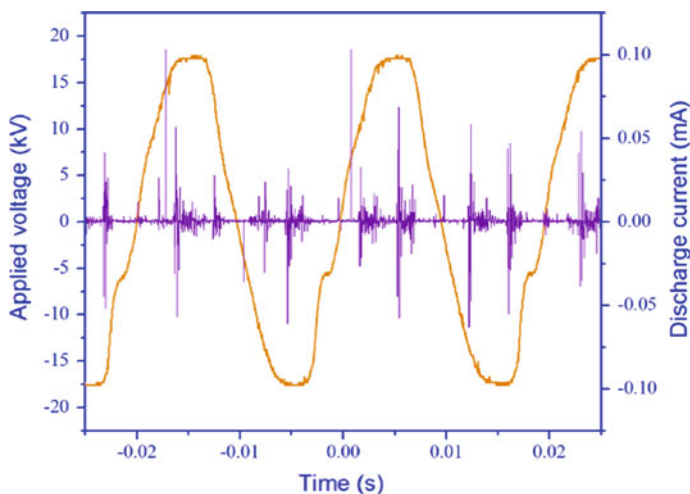


Fig. 13.16 Applied voltage and discharge current waveforms obtained in argon discharge

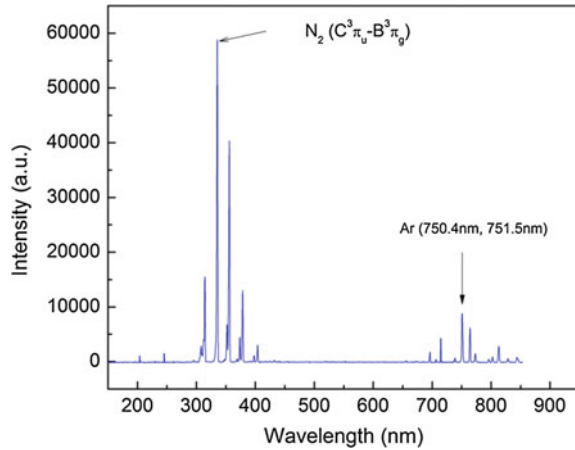
13.3.4.2 Optical Characterization

To understand the generation of reactive species in the plasma, it is important to measure the electron temperature and the density of the plasma. Conventional plasma diagnostics such as an electrostatic probe and a microwave interferometer are not applicable for atmospheric plasma [63]. Several attempts have been made to characterize atmospheric pressure DBD using OES technique to measure electron temperature and density [24, 47, 63–69].

OES analyzes the light emitted from the plasma. The light originates from the excited states decaying to lower energy levels in atoms and molecules due to various processes. OES can be used to identify the types of excited species present in the plasma. It can also be used to estimate the temperature of such species which is obtained from the analysis of the energy distributions of particles and their respective population. The transitions between electronic energy levels correspond to wavelength of light in ultraviolet to visible range. Therefore, the monochromator and photoelectron multiplier which are sensitive over a range of 200–900 nm can be employed. The resolution required for monochromator depends on the aim of the diagnostic. Normally, it is sufficient to resolve the vibrational structure of emission spectra of molecules with resolution of about 0.1 nm.

The typical optical emission spectrum in the range of 190–850 nm, recorded by a HORIBA Jobin Yvon UV–Vis Spectrometer, for DBD discharge in air is shown in Fig. 13.17. Its focal length is 140 mm and the grating used is 1200 per mm. Optical fiber with 100 μm diameter core and resolution of 2.3 nm is used to transmit the light from the source to the monochromator. The spectrum is recorded on the computer via SMA connector.

Fig. 13.17 Optical emission spectra of atmospheric DBD in air in the range of 190–850 nm



Measurement of electron temperature and electron density by line intensity ratio method

The electron temperature can be obtained by line intensity ratio method using the equation given below

$$\frac{R_1}{R_2} = \frac{I_1/I_2}{I_3/I_4} = \left(\frac{A_{pq}}{A_{xy}} \right) \left(\frac{g_p}{g_x} \right) \left(\frac{\lambda_{xy}}{\lambda_{pq}} \right) \left(\frac{A_{uv}}{A_{rs}} \right) \left(\frac{g_u}{g_r} \right) \left(\frac{\lambda_{rs}}{\lambda_{uv}} \right) \exp \left[- \frac{E_p - E_x - E_r + E_u}{kT_e} \right], \quad (13.3.3)$$

where R_1 is the ratio of the intensity of a pair of lines ($p \rightarrow q$) and ($x \rightarrow y$), assuming that ($p \rightarrow q$) is originated from neutral species (atom) while the transition ($x \rightarrow y$) is produced by singly ionized ion. Similarly, R_2 is the ratio of the intensity of another pair of lines ($r \rightarrow s$) and ($u \rightarrow v$), assuming that ($r \rightarrow s$) is originated from neutral species (atom) while the transition ($u \rightarrow v$) is produced by singly ionized ion. I is the intensity of the spectral line, λ_{ij} and A_{ij} are wavelength and transition probability, respectively. g_i is the statistical weight of the upper level, E_i is the energy of the upper level, k is the Boltzmann constant, and T_e is electron temperature. The values of λ and I are obtained from the optical emission spectra, and the values of A_{ij} , g_i , and E_i are obtained from the NIST atomic spectra database. Electron temperature T_e is then used to calculate the electron density n_e using Eq. (13.3.4).

$$n_e = 2 \left(\frac{I_1}{I_2} \right) \left(\frac{A_{xy}}{A_{pq}} \right) \left(\frac{g_x}{g_p} \right) \left(\frac{\lambda_{pq}}{\lambda_{xy}} \right) \left(\frac{2\pi m_e kT_e}{h^2} \right)^{3/2} \exp \left[\frac{E_i + E_p - E_x}{kT_e} \right] \quad (13.3.4)$$

Four suitable nitrogen lines, two for NII and two for NIII, are chosen from the spectrum and the electron temperature T_e is estimated using the line intensity ratio method.

Considering two NII lines with wavelengths 204.02 and 655.85 nm, and two NIII lines with wavelengths 245.21 and 378.57 nm, we obtain the intensities (from OES) and parameters from NIST Atomic Spectra Database which are listed in Table 13.1.

Substituting the above data in Eq. 13.3.3, we get

$$\frac{R_1}{R_2} = 0.506 \exp\left(\frac{2.78}{T_e}\right) \quad (13.3.5)$$

Taking different electron temperatures, we obtain the corresponding intensity ratio as given in Table 13.2.

Figure 13.18 is the graph plotted between electron temperature T_e and corresponding intensity ratio R_1/R_2 . This graph is used to determine the electron temperature using the value of R_1/R_2 obtained from the intensity ratio [70]. Since $R_1/R_2 = 9.16$, it corresponds to electron temperature 0.97 eV in Fig. 13.18.

The electron temperature T_e determined from above is then used to calculate the electron density n_e using Eq. 13.3.4. Considering two nitrogen lines NI (402.45 nm) and NII (397.98 nm), we obtain the intensities as given in Table 13.3 (from OES) and parameters from NIST Atomic Spectra Database.

Using the above data in Eq. 13.3.4 with electron temperature $T_e = 0.97$ eV and ionization potential of nitrogen $E_i = 14.53$ eV, we obtain the electron density $n_e = 3.46 \times 10^{17} \text{ m}^{-3}$.

Similarly, the electron temperature and electron density in argon/air mixture plasma can be obtained.

Measurement of Electron Density by Stark Broadening Method

One of the most reliable techniques to determine the electron number density is using the measured Stark broaden line profile of an isolated line of either neutral atom or singly charged ion. Stark broadening is caused by the Coulomb interaction between the radiator (in this case argon atom) and the charged particles present in the plasma.

The Stark broadening appearing due to collision of charged species is the primary mechanism influencing the width of Ar emission line. The stark broadened line is assumed to have the Lorentz profile. The electron number density (n_e) related

Table 13.1 Selected NII lines intensities (from OES) and parameters from NIST atomic spectra database

Nitrogen lines	Intensity (a. u.)	A_{ij}	g_i	E_i
NII (204.02 nm)	$I_1 = 1568.65$	$A_{pq} = 2.11 \times 10^6$	$g_p = 5$	$E_p = 21.62 \text{ eV}$
NII (655.85 nm)	$I_2 = 528.47$	$A_{xy} = 1.43 \times 10^6$	$g_x = 5$	$E_x = 41.73 \text{ eV}$
NIII (245.21 nm)	$I_3 = 1809.92$	$A_{rs} = 1.21 \times 10^7$	$g_r = 6$	$E_r = 23.26 \text{ eV}$
NIII (378.57 nm)	$I_4 = 5589.23$	$A_{uv} = 2.40 \times 10^6$	$g_u = 5$	$E_u = 40.59 \text{ eV}$

Table 13.2 Electron temperature for different values of R calculated in accordance with Eq. 13.3.5

Electron temperature (T_e)	R_1/R_2
0.9	11.1045
1	8.15387
1.1	6.33311
1.2	5.13052
1.3	4.29315
1.4	3.68507
1.5	3.22819
1.6	2.87514

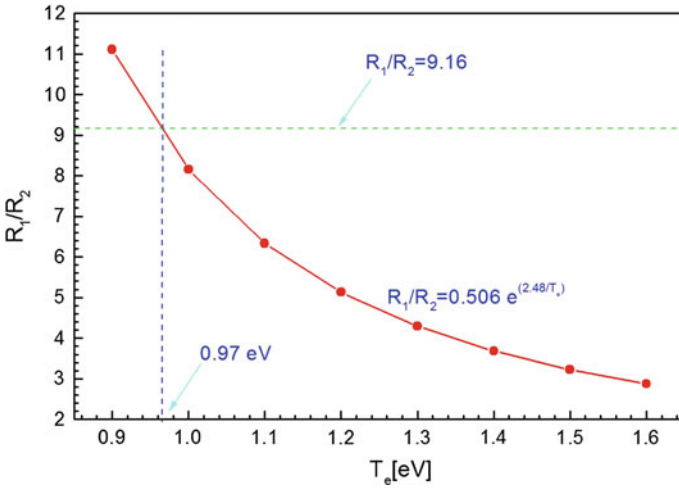


Fig. 13.18 Plot of R_1/R_2 as a function of T_e

Table 13.3 Spectroscopic constants for the two emission lines of nitrogen NI (402.45 nm) and NII (397.98 nm)

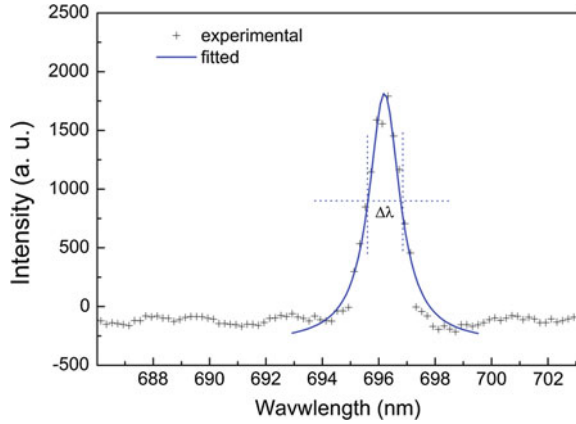
Nitrogen lines	Intensity (a. u.)	A_{ij}	g_i	E_i
NI (402.45 nm)	$I_1 = 1649.07$	$A_{pq} = 1.14 \times 10^6$	$g_p = 4$	$E_p = 10.71 \text{ eV}$
NII (397.98 nm)	$I_2 = 1478.17$	$A_{xy} = 7.79 \times 10^7$	$g_x = 5$	$E_x = 18.51 \text{ eV}$

to the full width at half maximum (FWHM) of the Stark broaden line is given by the expression [36].

$$\Delta\lambda_{\text{Stark}} = 2\omega \left[\frac{n_e}{10^{16}} \right] + 3.5 \alpha \left[\frac{n_e}{10^{16}} \right]^{1/4} \times \left[1 - \frac{3}{4} N_D^{-1/3} \right] \omega \left[\frac{n_e}{10^{16}} \right], \quad (13.3.6)$$

where ω is the electron impact width parameter (nm); α is the ion broadening parameter (nm); n_e is the electron density (cm^{-3}); N_d is the number of particles in the Debye sphere. The first term in Eq. (13.3.6) refers to the broadening due to the

Fig. 13.19 Emission line of argon/air plasma at 696.23 nm showing FWHM



electron contribution and the second term to the ion broadening contribution. Since the contribution of the ionic broadening is normally very small, therefore, it can be neglected and Eq. (13.3.6) can be reduced to a simple form:

$$\Delta\lambda_{\text{Stark}} = 2\omega \frac{n_e}{10^{16}} \quad (13.3.7)$$

Values of both ω and α for different temperatures are reported in [36]. Hence n_e can be expressed as

$$n_e = \left[\frac{\Delta\lambda_{\text{stark}}}{2 \times 10^{-11}} \right]^{\frac{3}{2}} \quad (13.3.8)$$

Equation 13.3.8 is an equation for determining the electron density in dielectric barrier discharge in argon by measuring the full width at half maximum (FWHM) of the emission line. The emission line of argon/air plasma at wavelength 696.23 nm is shown in Fig. 13.19.

The use of stark broadening of this line to estimate electron density in the discharge has also been reported in earlier papers [51, 61, 62].

The calculated value of electron density is $n_e = 6.04 \times 10^{16} \text{ cm}^{-3}$. This value is slightly higher than the results obtained by Balcon et al. [71] by Stark broadening on an argon line.

13.4 Application of DBD

The increasing application of DBD in industries is motivated by the possibility of treatment of pressure-sensitive objects and materials which cannot be treated using a low-pressure system. For example, treatment of living tissues, as in case of

medical treatment, is possible only with plasma devices which operate at atmospheric pressure.

Filamentary discharges controlled by dielectric barriers have been used for a long time in the fields of surface treatment and ozone production. This section will deal with some examples of DBD application for ozone generation, polymer surface modification, and plasma medicine. The surface modification of polymer material and the characterization of the modified polymer surface will be presented in more detail with special reference to contact angle and surface free energy analyses. The DBD was produced between electrodes with insulating layers of glass or polymer on the metal electrodes. An AC driving voltage of approximately 10 kV was used to create the discharge at DBD gap spacing of a few mm.

13.4.1 Ozone Generation

Many technical ozone generators make use of cylindrical discharge tube with diameter of about 20–50 mm and length of 1–2 m. Glass tubes are mounted inside stainless steel tube to form a narrow annular discharge space of about 0.5–1 mm. The high-voltage electrode is formed by a conductive coating (such as a thin aluminum film) on the inside of the glass tubes whereas the outer steel tubes serve as ground electrode. The preferred dielectric material is borosilicate glass. Other dielectrics such as ceramic tubes are also increasingly used. In advanced ozone generators, layered enamel coatings with optimized dielectric characteristics are also used. The ground electrode is cooled on the outside by a transverse water flow in a heat exchanger configuration. Since the efficiency of ozone formation decreases strongly with rising temperature, the ozone generator generally has narrow discharge gaps to ensure efficient heat removal. Previously, ozone generators were operated at line frequency. For smaller and low-cost ozone installation, this technique is still used. Modern high-power ozone generators use power semiconductors to generate square-wave currents with a frequency range of 0.5–5 kHz. Higher operating frequencies can deliver the desired power density at much lower operating voltages. The lower voltage results in less electrical stress on the dielectrics. Large ozone generators use several hundred discharge tubes and produce up to 100 kg of ozone per hour.

For industrial purposes, ozone is exclusively generated in large installations using dielectric barrier discharges. Ozone is a potent germicide and one of the strongest known oxidants. In many applications, it can replace chlorine thus causing less environmental concern. Although ozone itself is toxic, ozone treatment leaves no toxic residues in the medium that has to be treated or disposed of. The traditional application of ozone is for water treatment. About 100 years ago, it was realized that the germicidal and viricidal effects of ozone can provide safe drinking water in areas previously endangered by cholera. The first major ozone installation used in drinking water plant for disinfection was built around the beginning of the last century in Paris (1897) and Nice (1904), France; and in St. Petersburg, Russia

(1910). Although up to recently many countries have preferred chlorine for water treatment because of its lower cost, there is a strong tendency now to switch to ozone. The major targets for using ozone in water treatment are disinfection, color, odor, and iron removal. Another important growing large-scale use of ozone is in the paper industry. By combining oxygen, ozone, and hydrogen peroxide bleaches, pulp can be treated in a closed circuit without using chlorine. Extended reviews on ozone generation and their applications can be found in earlier works [72–75].

In this section, we present a small-scale ozone generator based on dielectric barrier discharge scheme. An attempt has been made to find out the optimum condition for higher ozone yield in coaxial cylindrical electrode. The schematic diagram of ozone generating system is shown in Fig. 13.20. Discharge from dielectric barrier was generated using high-voltage AC power supply operating at 50 Hz. The central electrode was made of a brass rod fixed inside a glass tube of thickness 1 mm. The gap between two glass layers was 2 mm. A sheet of aluminum wrapped outside of the tube acted as the outer electrode. The gas was passed inside the tube through the gap between the anode and the glass tube. It was supplied by air pump (ATEC Aquarium, AR-8500). The flow rate of air was 4 l/min. The concentration of ozone produced was measured by an ozone analyzer (Ozone Analyzer BMT 964, MESSTECHNIK GMBH Germany).

Effect of applied voltage on ozone concentration

Figure 13.21 shows the variation of ozone concentration as a function of applied voltage for a fixed air flow rate of 2 l/min at 2 mm gap with double barrier [77]. It is evident that ozone concentration increases as the applied voltage increases. It is due to the reason that the increase in voltage increases the electrical energy density, i.e., more energy transferred to the electrons, thereby increasing the possibility of collision of the air molecules in the chamber. However, supplied energy may not always be sufficient for recombination of ions, radicals, etc.

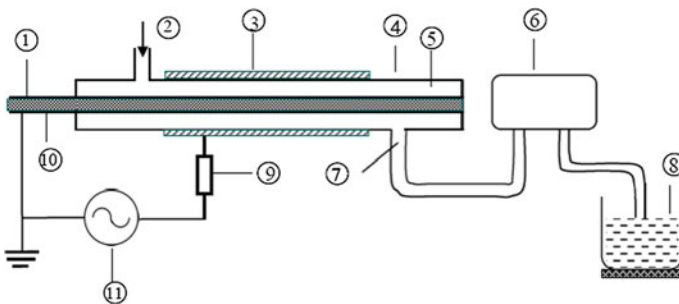


Fig. 13.20 Schematic diagram of ozonizer, 1 dielectric material, 2 gas inlet, 3 aluminum Sheet, 4 glass tube, 5 gap, 6 ozone analyzer, 7 outlet (mixture of air and ozone), 8 beaker with water, 9 resistance 10 k Ω , 10 central electrode, 11 power supply (18 kV, 50 Hz) [76]

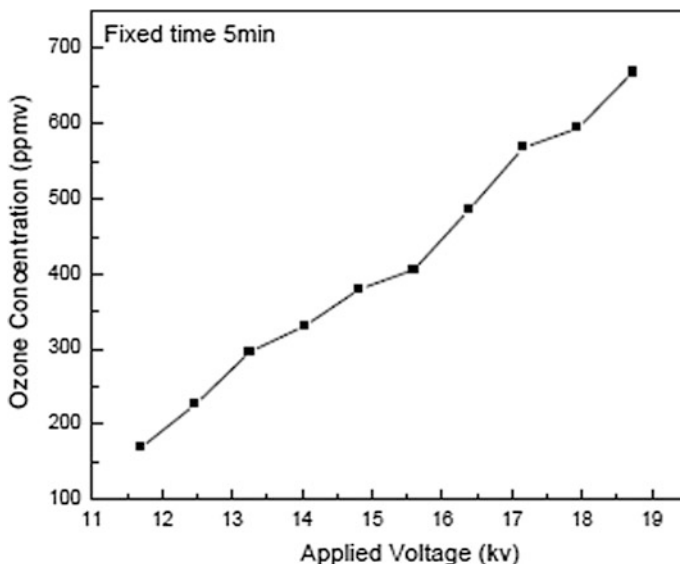


Fig. 13.21 Ozone concentration versus applied voltage for double barrier ozonizer with air flow rate of 2 l/min

13.4.2 Material Processing—Polymer Surface Modification

Polymers are used in a wide variety of applications including packaging and labeling, textile, stationary, automotive, laboratory equipment, etc. A low surface energy may be desirable in them for several applications, but for other applications it is a disadvantage, which has to be overcome [78]. As the surface energy of polymers is quite low, its surface properties such as hydrophilicity, adhesivity, and printability do not often meet the requirement for industrial applications. In order to extend its application range, different methods have been developed to modify its surface properties [79, 80]. Among them, atmospheric pressure nonthermal plasma treatment is a convenient and environmentally friendly way to obtain these modifications by introducing new chemical groups at the surface without affecting the bulk properties. However, most of such processes are conducted at low pressure and high frequency, which needs expensive vacuum equipment and batch treatments, and therefore it is difficult to apply these processes to large-scale objects, especially under the condition of continuous treatment. This environmentally friendly dry treatment can modify the surface properties of materials without changing the chemical and physical bulk properties [81].

The result of atmospheric pressure dielectric barrier discharge is similar to that obtained in low-pressure discharges, that is, to produce a substantial increase of surface free energy. It is reported that the surface free energy of untreated polymers changes from 20–30 to 50–70 mJ/m² after the treatment by atmospheric pressure

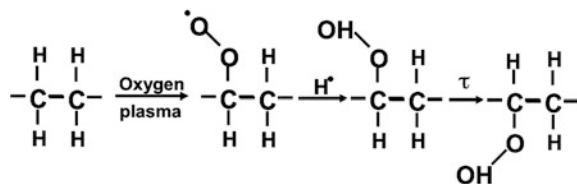
DBD (APDBD) [82] making material surface more wettable. APDBD thus enhances the adhesion, printability, and dye uptake of material surface. Recent investigations also include the upgrading of wool and textiles and the plasma treatment of insulated wires and cables.

During surface activation, radicals formed in the plasma disrupt chemical bonds in the surface layer causing the formation of new species with different properties. This results in a modification of the near-surface region without changing the desirable bulk properties of the material. In air plasmas, the active species are identified as oxygen atoms resulting in the buildup of oxygenated carbon centers in the surface layer.

Several studies carried out in plasma surface modification had shown that the modified surface is not stable for long time [8, 83, 84]. The treated polymer recovers a significant fraction of its hydrophobic property with the storage time after treatment. Figure 13.22 shows a schematic representation of a possible situation during surface modification of a polymer containing only carbon and hydrogen atoms such as polyethylene exposed to oxygen plasma. It also shows the mechanism responsible for the hydrophobic recovery (aging) in plasma-treated polymers. Inelastic collisions, mainly involving energetic electrons in the discharge and species on the polymer surface, can result in chemical bonds breakage creating free radicals in the material. Reactions between free radicals and atomic oxygen can add peroxides to the surface as shown in Fig. 13.22. Chemical reactions involving peroxides and species, such as atomic hydrogen originated from the polymer or atmospheric contaminants, can incorporate hydrophilic groups to the polymer surface. This modification enhances the surface energy.

The experimental DBD setup used for polymer treatment is shown in Fig. 13.23. For the discharge, two rectangular copper electrodes with dimensions 5 cm \times 3.5 cm \times 1 cm are used. The lower electrode is covered by a polycarbonate (PC) plate with dimensions 10 cm \times 8 cm \times 0.2 cm as a dielectric barrier, separated by a gap between two electrodes. The discharge was generated via line frequency (50 Hz), high-voltage (maximum peak-to-peak value of 50 kV) power supply. The plasma surface treatment was performed by placing the polymer samples with dimensions 3 cm \times 2.5 cm on the dielectric material, i.e., the polycarbonate (PC) plate in between the two electrodes at room temperature. Dry ambient air and a mixture of air and argon are used as plasma gas. Argon with a flow rate of about 2 l per minute is used in case of air and argon mixture. The plasma treatment time varied from 5 to 60 s. Surface treatments are performed by setting the electrode gap to 3.5 mm with applied voltage 13 kV rms and ballast

Fig. 13.22 Schematic representation of a possible mechanism responsible for the hydrophobic recovery in plasma treated polymer [83]



resistor 20 M Ω . Commercially available four different types of polymer films, namely high-density polyethylene (HDPE), polyethylene terephthalate (PET), polypropylene (PP), and polyamide 6,6 (PA), from Goodfellow Cambridge Limited, UK with dimensions 3 cm \times 2.5 cm were used as samples for plasma treatment. Before the DBD plasma treatment, the samples were washed in isopropyl alcohol and then washed in distilled water, and ultrasonicated for 10 min and dried at room temperature.

Surface characterization of plasma-treated polymers

Polymer samples before and after the treatment are studied using contact angle measurements, surface free energy calculations, scanning electron microscopy (SEM), and atomic force microscopy (AFM).

Measurement of contact angle of liquid with the solid surface permits a rapid and qualitative evaluation of surface free energy of polymers. Analysis of the surface free energy of the untreated and plasma-treated samples has been made by measuring its surface free energy (γ), its dispersion part (γ^{LW}), and its acid–base part (γ^{AB}) along with the electron–donor component (γ^+) and the electron–acceptor component (γ^-) of the acid–base interaction.

In case of sessile drop method, values of contact angles are recorded for a few test liquids with well-defined surface tension and its components described as polar part and dispersive part. The interaction between a single droplet and tested surface in the most general form can be expressed by Young's equation [83–85]:

$$\gamma_S = \gamma_{SL} + \gamma_L \cos \theta, \quad (13.4.1)$$

where γ_S is the unknown surface free energy (SFE) of tested surface, γ_{SL} is the surface tension of solid–liquid interface, γ_L is the surface tension of a test liquid, and θ is the contact angle between the solid and the test liquid as shown in

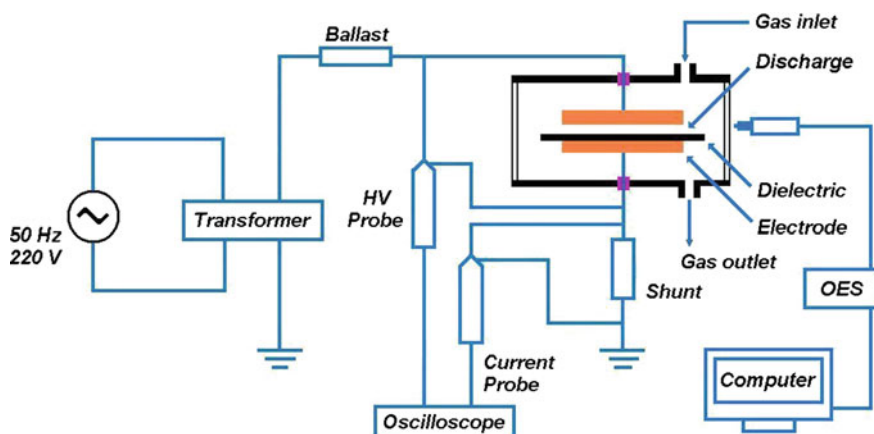


Fig. 13.23 Schematic diagram of the experimental setup

Fig. 13.24 Schematic diagram contact angle and interfacial tensions of three surfaces

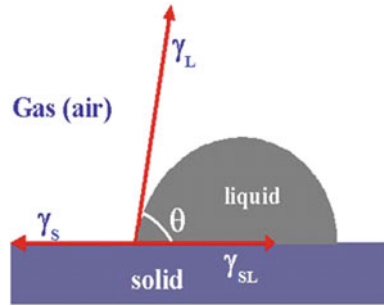


Fig. 13.24. It comes out from Eq. (13.4.1) that the difference $\gamma_s - \gamma_{SL}$ can be obtained from the experimental values of γ_L and θ .

On the other hand, the work of adhesion for a liquid and a solid in contact, W_{SL} , is given, according to Young–Dupre equation by Refs. [78, 86–90],

$$W_{SL} = \gamma_s + \gamma_L - \gamma_{SL} \quad (13.4.2)$$

In addition, it has been proposed that two different interactions of the work of adhesion W_{SL} can be obtained: W_{SL}^{LW} derived from London dispersive forces, i.e., from apolar or dispersive or Lifschitz–van der Waals (LW) interactions and W_{SL}^{AB} derived from nondispersive interactions, i.e., from acid–base (AB) interactions or electron–acceptor/electron–donor interactions (deriving from hydrogen bonding, dipole–dipole interactions, etc.) [91]:

$$W_{SL} = W_{SL}^{LW} + W_{SL}^{AB}$$

The total surface free energy can be written as [89]

$$\gamma_s = \gamma^{LW} + \gamma^{AB}$$

W_{SL}^{LW} can be expressed by the geometric mean of the dispersion components [88]:

$$W_{SL}^{LW} = 2(\gamma_s^{LW} \cdot \gamma_L^{LW})^{1/2}$$

However, the acid–base interactions do not obey the geometric mean combining rule because they are complementary rather than symmetrical. For this reason, the acid–base term, γ^{AB} , should be split into an electron acceptor surface parameter, γ^+ , and an electron donor surface parameter, γ^- , in such a way that $\gamma^{AB} = 2(\gamma^+ \cdot \gamma^-)^{1/2}$. The acid–base contribution to the work of adhesion between the solid and the liquid is thus given by,

$$W_{SL}^{AB} = 2(\gamma_S^+ \cdot \gamma_L^-)^{1/2} + 2(\gamma_S^- \cdot \gamma_L^+)^{1/2}$$

For the total work of adhesion, the sum of LW and AB contributions is given by,

$$W_{SL} = 2(\gamma_S^{LW} \cdot \gamma_L^{LW})^{1/2} + 2(\gamma_S^+ \cdot \gamma_L^-)^{1/2} + 2(\gamma_S^- \cdot \gamma_L^+)^{1/2} \quad (13.4.3)$$

From Eqs. (13.4.1), (13.4.2), and (13.4.3), we get

$$\gamma_L(1 + \cos \theta) = 2(\gamma_S^{LW} \cdot \gamma_L^{LW})^{1/2} + 2(\gamma_S^+ \cdot \gamma_L^-)^{1/2} + 2(\gamma_S^- \cdot \gamma_L^+)^{1/2},$$

which allows the determination of LW and AB components of the surface tension of a solid surface from contact angle measurements of three testing liquids with known values of the surface tension components. Table 13.4 shows the surface tension and its polar and dispersive part of three test liquids used for the contact angle measurements.

Contact angle measurement and wettability

Static contact angle measurements are made before the treatment and immediately after the treatment by dropping 4 μ l of distilled water (H₂O), glycerol (C₃H₈O₃), and diiodomethane (CH₂I₂) on the surface. Different liquid drops on the polymer surface were imaged using CCD camera and the contact angles were measured by ramé-hart Model 200 contact angle goniometer. The values of the static contact angle were the average of three measured values. It is seen that a rapid decrease in the static water contact angle takes place with the treatment time up to 10 s which shows that a strong increase of wettability in the polymer surface is induced by DBD treatment. After 10 s of DBD treatment in air, the static water contact angle of untreated HDPE, PET, PP, and PA changed from (i) 92.8° to 63.7°, (ii) 76.7° to 44.8°, (iii) 93.7° to 76.4°, and (iv) 51.2° to 32.4°, respectively. Similarly, after 10 s of DBD treatment in argon/air mixture, the static water contact angle of untreated HDPE, PET, PP, and PA changed from (i) 92.8° to 51.4°, (ii) 76.7° to 36.5°, (iii) 93.7° to 66.0°, and (iv) 51.2° to 25.2°, respectively. This shows that DBD treatment in argon/air mixture decreased the static water contact angle more than DBD treatment in air with the same treatment time which clearly proved that a significant increase of wettability in the polymer surface can be induced by introducing a small amount of argon in the discharge gas environment. Figure 13.25

Table 13.4 Surface tension and its polar and dispersive part of three test liquids used for the contact angle measurements

Liquid	Total (γ_L)	Dispersive (γ_L^{LW})	Polar (γ_L^{AB})	Polar + (γ_L^+)	Polar - (γ_L^-)
Water	72.8	21.8	51.0	25.5	25.5
Glycerol	63.9	37.5	26.4	3.9	57.4
Diiodomethane	50.8	50.8	0	0	0

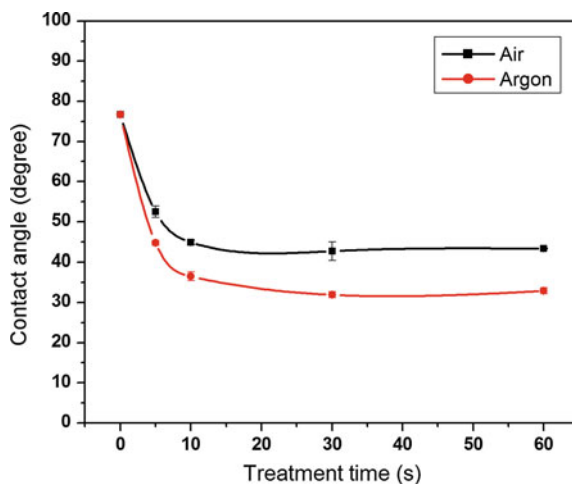
shows the variation of the static water contact angle on the surface of the PET film with DBD treatment time, both in air and in argon/air mixture. The results show that for PET film the treatment time longer than 10 s is not helpful as the decrease in contact angle becomes stable.

From the results mentioned above, it has been verified that atmospheric pressure dielectric barrier discharge (DBD) can be successfully used for the surface hydrophilization. It has been shown that different polymer surfaces can be treated to achieve high hydrophilicity with relatively short treatment time (up to 10 s). Longer exposure time do not cause significant changes in static contact angle values which means that saturation of plasma effect occurs. The contact angles are measured over an extended area of the treated sample and show a dispersion lower than 2.5° which is within the limit of experimental error. This implies that the surface treatment is uniform despite the fact that the discharge consists of a series of micro-discharges randomly distributed over the electrode/sample surface. The steep diminution of the contact angles on treated samples compared to the untreated one shows the significantly increased wettability induced by DBD even after such short treatment times. This behavior can be attributed to strong surface oxidation. The molecular oxygen in the contacting air is activated, ionized, and dissociated in the discharge to give extremely reactive oxygen species that react readily with the substrate surface.

Surface free energy results

The static contact angles between the three test liquids and different polymers are measured in order to determine the total surface free energy using sessile drop technique and three-liquid model. The surface free energy is calculated from Young–Dupre equation using the contact angle. It is seen that after 10 s of DBD treatment in air, the surface free energy of untreated HDPE, PET, PP, and PA changed from (i) 35.0 to 43.6 mJ/m^2 , (ii) 44.5 to 53.6 mJ/m^2 , (iii) 36.7 to 43.5 mJ/m^2 , and (iv) 49.4 to 54.2 mJ/m^2 , respectively. Similarly, after 10 s of DBD

Fig. 13.25 Variation of water contact angle with treatment time (PET)

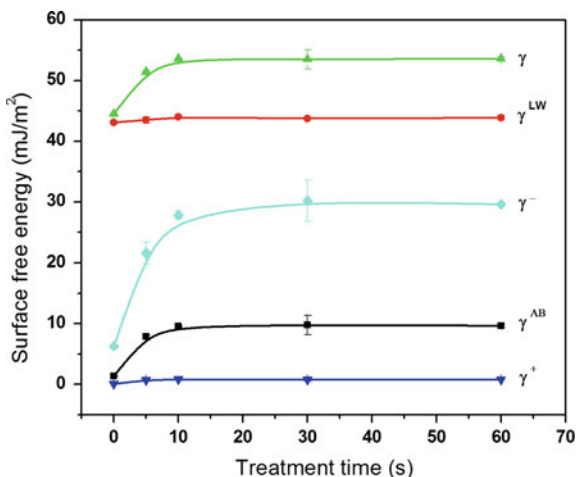


treatment in argon/air mixture, the surface free energy of untreated HDPE, PET, PP, and PA changed from (i) 35.0 to 48.2 mJ/m², (ii) 44.5 to 55.4 mJ/m², (iii) 36.7 to 42.8 mJ/m², and (iv) 49.4 to 61.0 mJ/m², respectively. Further treatment of polymers after 10 s, for both ambiances, does not lead to any significant changes in the surface free energy. DBD treatment in argon/air mixture increases the surface free energy more than DBD treatment in air. Figure 13.26 shows the dependence of surface free energy and its components on treatment time of PET in air plasma.

Scanning electron microscopy (SEM)

In order to compare the polymer surface modifications in air plasma and argon/air mixture plasma, SEM imaging is performed using Leo 500 scanning electron microscope for surface topography characterization. Figure 13.27a shows the SEM micrograph of untreated sample of PET and profile of a water droplet on the surface, showing measured contact angle of 76.7°. Figure 13.27b shows the SEM micrograph of PET sample that has been treated in air plasma for 60 s and profile of a water droplet on the surface, showing measured contact angle of 43.2°. Figure 13.27c shows the SEM micrograph of PET surface treated in argon/air mixture plasma for 60 s and profile of a water droplet on the surface, showing measured contact angle of 32.9°. The topography of the treated polymers appears to be quite different from the untreated one. It is seen that the surface of the air plasma-treated polymer has slightly increased surface roughness compared to the untreated polymer surface. The surface of the argon/air mixture plasma-treated polymer, however, is changed drastically with highly increased surface roughness compared to both the untreated and air plasma-treated polymers. This is caused by the dominant etching effect of the argon plasma treatment. The main species in the plasma which are responsible for the etching effect are positive ions and photons,

Fig. 13.26 Variation of surface free energy and its components with treatment time for PET in air plasma. γ is the surface free energy, γ^{LW} is its dispersion part, and γ^{AB} is its acid–base part. γ^+ is the electron–donor component and γ^- is the electron–acceptor component of the acid–base interaction



with the ability of breaking primary chemical bonds and introducing cross-linking. It is quite interesting to note that the roughness of the polymer treated in argon/air mixture plasma is more prominent than in the case of air plasma treatment. The air plasma has only a slight effect on the topography of the polymers.

Atomic force microscopy (AFM)

In order to compare the polymer surface modifications in air plasma and argon/air mixture plasma, AFM imaging is also performed using Nanoscope III SPM atomic

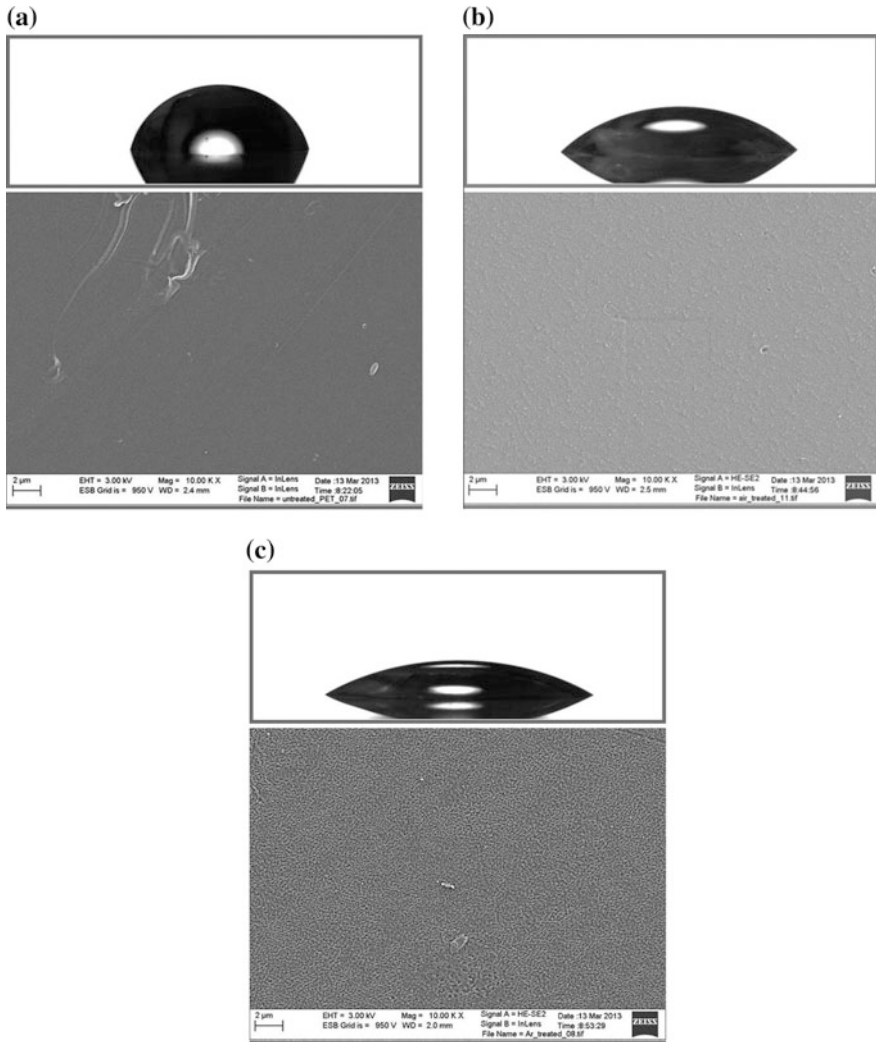


Fig. 13.27 SEM image and profile of a water droplet on the surface of untreated PET (a), treated in air plasma for 60 s (b) treated in argon/air mixture plasma for 60 s (c)

force microscope for surface morphology characterizing of polymer. It is seen that the argon/air mixture plasma-treated polymer samples are most pronounced than untreated and air plasma-treated samples. It is known that the argon plasma does not allow incorporation of new chemical species into the polymer chains. Despite this, argon/air plasma-treated surface gets much more oxygen-containing polar groups than the untreated and air plasma-treated surface. This phenomenon can be explained as argon has lower breakdown potential than air. The blending of it can make the discharging more symmetrical which can lead to ample plasma ionization. Figure 13.28a shows the 2-D AFM image of untreated sample of HDPE and profile of a water droplet on the surface, showing measured contact angle of 92.8° . The morphology of the untreated HDPE appears comparatively smooth. Figure 13.28b shows the 2-D AFM image of HDPE sample that has been treated in air plasma for 60 s and profile of a water droplet on the surface, showing measured contact angle of 54.0° . As can be seen from the figure, the surface of the air plasma-treated HDPE has only slightly increased surface roughness compared to the untreated HDPE. Figure 13.28c shows the 2-D AFM of HDPE surface treated in argon/air mixture plasma for 60 s and profile of a water droplet on the surface, showing measured contact angle of 46.1° . It is also clearly seen that the surface of the argon/air mixture plasma-treated HDPE has been changed drastically with highly increased surface roughness compared to both the untreated HDPE and air plasma-treated HDPE. As can be seen, the air plasma has only a slight effect on the morphology of HDPE. These results can also be observed in 3-D AFM images presented in Figs. 13.29a, b and 13.30.

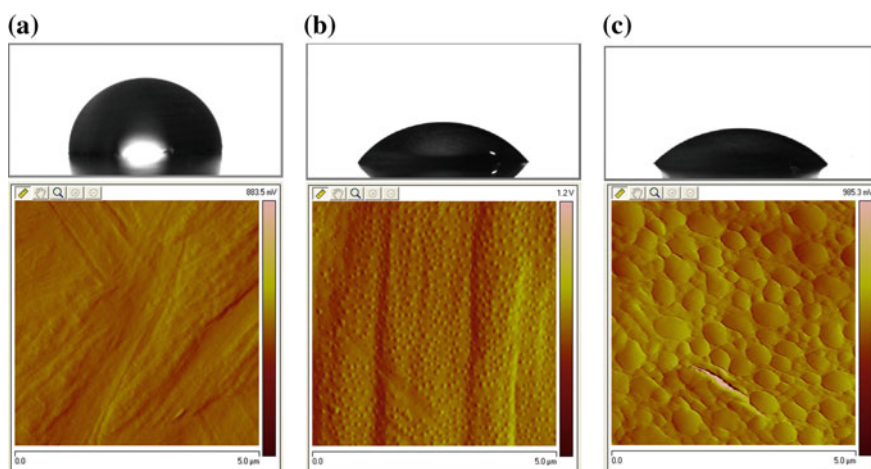


Fig. 13.28 a 2-D AFM image of untreated HDPE; b AFM image of HDPE treated in air plasma for 60 s; and c AFM image of HDPE treated in argon/air mixture plasma for 60 s

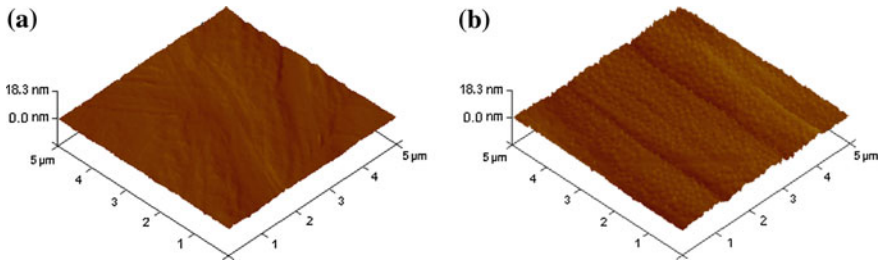


Fig. 13.29 3-D AFM image of **a** untreated HDPE and **b** HDPE surface treated in air plasma for 60 s

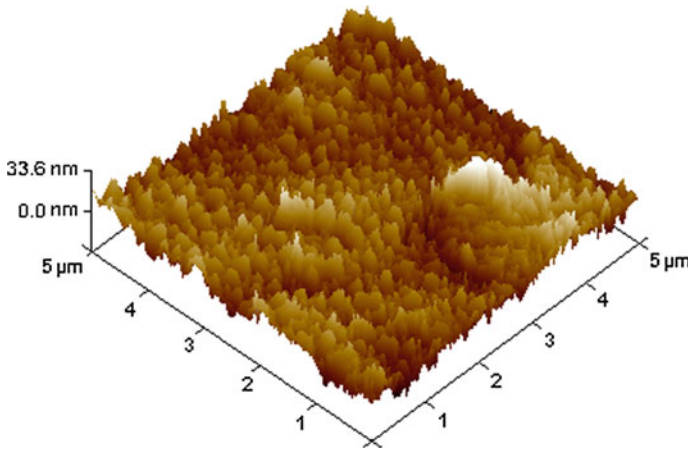


Fig. 13.30 3-D AFM image of HDPE surface treated in argon/air mixture plasma for 60 s

13.4.3 Plasma Medicine

Some of the earlier applications of plasma in medicine relied mainly on the thermal effects of plasma. Heat and high temperature have been exploited in medicine for a long time for the purpose of tissue removal, sterilization, and cauterization. Recently, research on applications of plasma in medicine has shifted to the exploitation of nonthermal effects [43]. Nonthermal atmospheric pressure plasma sources offer efficient means for the production of chemically active radicals under low thermal loading conditions. The ability of these devices to operate outside vacuum chambers not only reduces the overall operation and installation costs, but also permits the treatment of mechanically sensitive materials, such as biomaterials and human tissues [92]. Nonequilibrium plasmas are found to be nondestructive to tissue, safe, and effective in inactivation of various parasites and foreign organisms [43]. Various types of atmospheric pressure plasma sources have been designed for

a wide range of biomedical and industrial applications, like plasma needle, floating-electrode DBD, microhollow cathode discharge air plasma jet, and various other forms of plasma jets [12, 43, 77, 92–96]. Atmospheric pressure plasma jets have been established as suitable sources of low-temperature and nonequilibrium atmospheric pressure plasmas. The plasma jet devices generate plasma plumes in open space rather than in confined discharge gaps only. Thus, they can be used for direct treatment and there is no limitation on the size of the object to be treated [77].

As an example, a recent work on the application of atmospheric pressure plasma jet for the inactivation of prokaryotic cells (*Escherichia coli*, *Staphylococcus aureus*, etc.) and eukaryotic cells (*Candida albicans*, *Saccharomyces cerevisiae*, etc.) to obtain $>4 \log_{10}$ reduction in *E. coli* and <2000 cells reduction in eukaryotic microalgae *C. vulgaris* is briefly discussed in this section.

An atmospheric pressure single-electrode argon/oxygen plasma jet was generated between a high-voltage (3.5 kV, 27 kHz) electrode and the surrounding room air for treatment of the cells. The micro-plasma jet device operated with an electrical power less than 10 W exhibited a long plasma jet of about 8.0 cm with temperature near 300 K, not causing any harm to human skin. Optical emission spectra measured in the range of 200–900 nm showed that various reactive species such as O, OH, N_2^+ , Ar^+ , etc., are present in the plasma plume. The schematic diagram of the experimental setup used in the present work is depicted in Fig. 13.31.

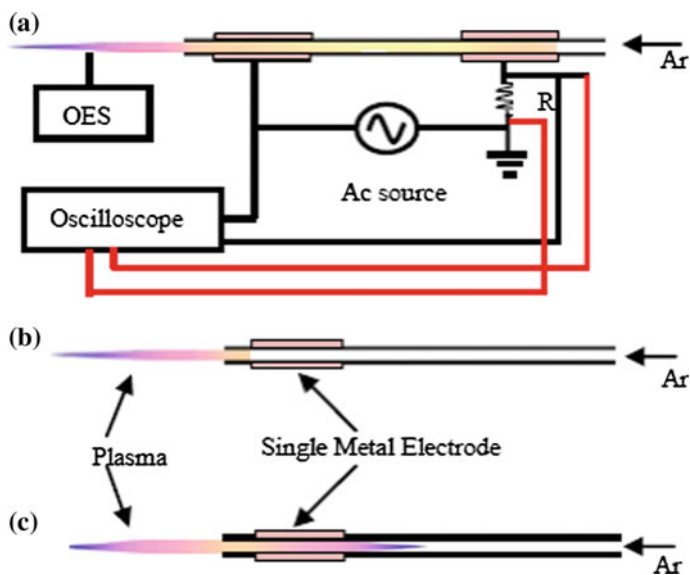


Fig. 13.31 Schematic diagram of the experimental setup used for the treatment of the cells. The discharge was generated by a high-voltage power supply with $V_{ap} = 3.5$ kV, $f = 27$ kHz and gas flow rate $Q = 2$ l/min

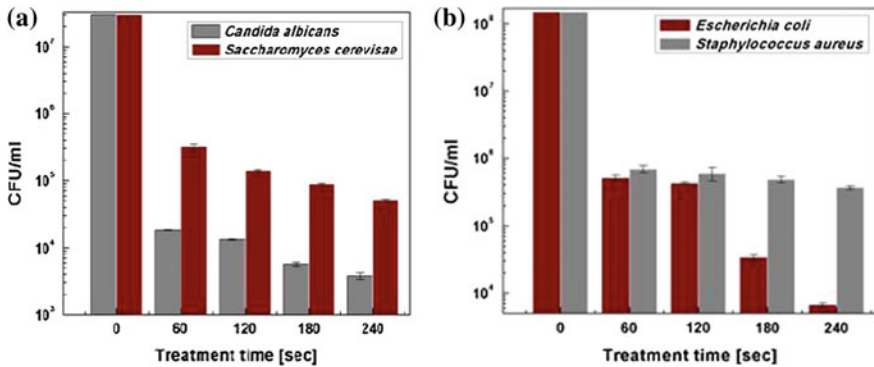


Fig. 13.32 CFU in **a** eukaryotic yeast cells **b** prokaryotic bacteria cells as a function of treatment time in APPJ. The treatments were carried out at distance of 3.5 cm from nozzle in 12 well plates [77]

In order to demonstrate that plasma species are solely responsible for inactivating living cells, the effect of plasma jet in pH and temperature of cell culture medium was also investigated.

Colony Forming Unit (CFU) analysis was done to investigate the number of dead cells and number of viable (live) cells. Treated and untreated samples were diluted by 10–10⁴ times. 100 μ l of diluted sample was spread on Plate Count Agar (PCA) using sterile bent glass rod. Then, the samples were incubated for 24 h at 37^o C. After incubation, viable colony of microbes were counted using Quebec Colony Counter (QCC). By spread plate technique, viable cell colony was counted using QCC. More than 4 log reductions were observed in *E. coli*, *Staphylococcus*, *C. albicans*, and *S. cerevisiae*. In eukaryotic microalgae, more than 2000 cells were killed by jet at a maximum treatment time of 240 s, as measured using UV–Vis spectrophotometer taking into account the absorbance of the cell suspension before and after treatment.

Figure 13.32a, b indicates that plasma jet is responsible for the killing of prokaryotic and eukaryotic cells. The inactivation and killing of both prokaryotic and eukaryotic cells increased as the treatment time increased with argon as carrier gases.

13.5 Summary

An overview of low-temperature, nonthermal plasma with focus on dielectric barrier discharge has been presented. Low-pressure gaseous discharges which can be generated by DC, RF, or MW power sources have been briefly described before introducing different types of atmospheric pressure plasmas. This chapter mainly

focused on atmospheric pressure DBD, its generation, characterization, and application in some selected fields.

Although the field of low-pressure plasma has been studied for quite a long time, the field of atmospheric pressure plasma is still very young. In the past few decades, new and interesting applications are emerging rapidly and hence interest in this field of research is growing in the same rate. One of the most challenging topics of research for the coming years will be to generate a larger volume of stable and homogenous plasma at atmospheric pressure so that material processing which originally used to be carried out in low pressure could be possible at atmospheric pressure thereby significantly reducing the cost of installation, operation, and maintenance. This will demand a better understanding of the discharge process at atmospheric pressure mainly, the nature of micro-discharges and the associated plasma chemical reactions in such systems. Numerous attempts have been made in this direction by improving existing diagnostics tools and also by introducing new methods. This will not only increase our understanding but will also pave the way for development of new applications of these cost-effective plasmas.

Acknowledgements The authors would like to thank Dr. Raju Bhai Tyata, Dr. Rajendra Shrestha, Mr. Amit Shrestha, Ms. Arati Khadgi, Ms. Rita Bhatta, and Mr. Jyoti Gurung for their contribution in this work. The authors would also like to thank Prof. Andrzej Huczko from Department of Chemistry, University of Warsaw, Poland for AFM and SEM analysis. We would also like to thank Mr. Suraj Sharma, for his assistance in drawing the schematic diagrams of plasma systems.

References

1. U. Kogelschatz, B. Eliasson, W. Egli, From ozone generators to at television screens: history and future potential of dielectric-barrier discharges. *Pure Appl. Chem.* **71**(10), 1828 (1999)
2. J. Janca, P. Stahel, J. Buchta et al., A plasma surface treatment of polyester textile fabrics used for reinforcement of car tires. *Plasmas Polym.* **6**(1/2), (2001)
3. P. Stahel, J. Janca, D.P. Subedi, Surfaceactivation of non-fabricated polymeric textile by means of low temperature plasmas at atmosphericpressure. *Czechoslovak J. Phys.* **52** (2002)
4. D.P. Subedi, L. Zajickova, V. Bursikova et al., Surface modification of polycarbonate (bisphenol A) by low pressure rf plasma. *Him. J. Sci.* **1**(2), 115–118 (2003)
5. S. Starostin, E. Aldea, H. de Vries et al., Application of atmospheric pressure glow discharge (APGD) for deposition of thin silica-like films on polymeric webs, in *28th ICPiG*, Prague, Czech Republic, 2007
6. Y. Yin, L. Dongping, L. Dongming et al., Surface properties of silicon oxide films deposited using low-pressure dielectric barrier discharge. *Appl. Surf. Sci.* **18628**, 1–5 (2009). doi:[10.1016/j.apsusc.2009.04.142](https://doi.org/10.1016/j.apsusc.2009.04.142)
7. V. Bursikova, L. Zajickova, P. Dvorak et al., Plasma enhanced chemical vapor deposition of silicon incorporated diamond like carbon films, in *Proceeding XVth Europhysics Conference on Atomic and Molecular Physics of Ionized Gases, Miscolc-lillafured*, Hungary 2000, pp. 408–409
8. L. Zajickova, V. Bursikova, V. Perina et al., Plasma modifications of polycarbonates. *Surf. Coat. Technol.* **142–144**, 449–454 (2001)

9. L. Zajickova, D.P. Subedi, V. Bursikova et al., Study of argon plasma treatment of polycarbonate substrate and its effect on film deposition. *Acta Phys. Slovaca*. **53**(6), 489–504 (2003)
10. G. Fridman, G. Friedman, A. Gutsol et al., Applied plasma medicine. *Plasma Process. Polym.* **5** (2008)
11. M.S. Bell, B.K.T. Kenneth, G.L. Rodrigo et al., Carbon nanotubes by plasma-enhanced chemical vapor deposition. *Pure Appl. Chem.* **78**(6), 1117–1125 (2006)
12. P. Rajasekaran, P. Mertmann, N. Bibinov et al., DBD plasma source operated in single-filamentary mode for therapeutic use in dermatology. *J. Phys. D Appl. Phys.* **42** (2009). doi:[10.1088/0022-3727/42/22/225201](https://doi.org/10.1088/0022-3727/42/22/225201)
13. G. Borcia, C.A. Anderson, N.M.D. Brown, Dielectric barrier discharge for surface treatment: application to selected polymers in film and fibre form. *Plasma Sources Sci. Technol.* **12**, 335–344 (2003)
14. K. Okazaki, T. Nozaki, Ultrashort pulsed barrier discharges and Applications. *Pure Appl. Chem.* **74**(3), 447–452 (2002)
15. A.P. Napartovich, Overview of atmospheric pressure discharges producing non-thermal plasma. *Plasmas Polym.* **6**(1–2), (2001)
16. V.I. Gibalov, G.J. Pietsch, Dynamics of dielectric barrier discharges in different arrangements. *Plasma Sources Sci. Technol.* **21** (2012)
17. A. Schutze, J.Y. Jeong, S.E. Babayan et al., The atmospheric-pressure plasma jet: a review and comparison to other plasma sources. *IEEE Trans. Plasma Sci.* **26**(6), (1998)
18. B. Graham, Technological plasmas. *Phys. World*. 31–36 (2001)
19. E. Stoffels, W. Stoffels, *Electrons, Ions and Dust in a Radio Frequency Discharge*, (Eindhoven, 1994)
20. M. Konuma, *Film Deposition by Plasma Techniques*, (Stuttgart, 1991)
21. A.M. Howatson, *An Introduction to Gas Discharges* (Pergamon Press, Frankfurt, 1976)
22. L. Zajickova Thin films prepared by radio frequency PECVD. PhD thesis, Department of Physical Electronics, Masaryk University, Brno, Czech Republic, 1999
23. J.L. Cecchi, *Introduction to Plasma Concepts and Discharge Configurations*, (Noyes Publications, New Jersey, 1990), pp. 14–69
24. S.Y. Moon, J. Han, W. Choeb, Control of radio-frequency atmospheric pressure argon plasma characteristics by helium gas mixing. *Phys. Plasmas*. **13** (2006)
25. Y.A. Lebedev, Microwave discharges: generation and diagnostics. *J. Phys. Conf. Ser.* **257** (2010). doi:[10.1088/1742-6596/257/1/012016](https://doi.org/10.1088/1742-6596/257/1/012016)
26. H. Conrads, M. Schmidt, Plasma generation and plasma sources. *Plasma Sources Sci. Technol.* **9**, 441–454 (2000)
27. A.R. Hoskinson, J. Hopwood, A two-dimensional array of microplasmas generated using microwave resonators. *Plasma Sources Sci. Technol.* **21** (2012)
28. K. Tanaka, M. Kogoma, Application of spray-type atmospheric pressure glow plasma reactor: ashing of organic compounds. *Plasmas Polym.* **6**(1–2), (2001)
29. L. Peng, Z. Ru-juan, W. Xiac-hui et al., An experimental study on atmospheric pressure glow discharge in different gases. *Plasma Sci. Technol.* **4**(3), (2002)
30. G. Chen, S. Chen, M. Zhou et al., The preliminary discharging characterization of a novel APGD plume and its application in organic contaminant degradation. *Plasma Sources Sci. Technol.* **15**, 603–608 (2006). doi:[10.1088/0963-0252/15/4/002](https://doi.org/10.1088/0963-0252/15/4/002)
31. Z. Buntat, I.R. Smith, N.A.M. Razali, Ozone generation using atmospheric pressure glow discharge in air. *J. Phys. D: Appl. Phys.* **42** (2009)
32. L. Mangolini, C. Anderson, J. Heberlein et al., Effects of current limitation through the dielectric in atmospheric pressure glows in helium. *J. Phys. D Appl. Phys.* **37**, 1021–1030 (2003)
33. M. Goldman, A. Goldman, R.S. Sigmond, The corona discharge, its properties and specific uses. *Pure Appl. Chem.* **57**(9), 1353–1362 (1985)
34. Y.S. Akishev, G.I. Aponin, V.B. Karal'nik, Phenomenology of a high-current negative point-to-plane corona in nitrogen. *Plasma Phys. Rep.* **30**(9), 779–787 (2004)

35. L. Cernakova, D. Kovacik, A. Zahoranova et al., Surface modification of polypropylenenon-wovenfabrics by atmospheric-pressure plasma activation followed by acrylic acid grafting. *Plasma Chem. Plasma Process.* **25**(4), (2005)
36. B. Dong, J.M. Bauchire, J.M. Povesle et al., Experimental study of a DBD surface discharge for the active control of subsonic airflow. *J. Phys. D Appl. Phys.* **41** (2008)
37. U. Kogelschatz, Collective phenomena in volume and surface barrier discharges. *J. Phys.: Conf. Ser.* **257** (2010) 012015, in *25th Summer School and International Symposium on the Physics of Ionized Gases—SPIG 2010*, IOP Publishing, 2010
38. M. Laroussi, X. Lu, V. Kolobov et al., Power consideration in the pulsed dielectric barrier discharge at atmospheric pressure. *J. Appl. Phys.* **96**(51), (2004)
39. N. Balcon, A. Aanesland, R. Boswell, *Pulsed rf Discharge, Glow and Filamentary Mode At atmospheric Pressure in Argon*, vol. 16, (IOP Publishing Ltd., 2006)
40. https://www.plasma-universe.com/Electric_glow_discharge (14 Sept 2016)
41. Y. Ando, X. Zhao, Synthesis of carbon nanotubes by arc discharge method. *New Diam. Front. Carbon Technol.* **16**(3), (2006)
42. C. Fanara, L. Vilarinho, Electrical characterization of atmospheric pressure arc plasmas. *Eur. Phys. J. D* **28**, 241–251 (2004)
43. A. Fridman, *Plasma Chemistry* (Cambridge University Press, Cambridge, 2008)
44. A. Chirokov, A. Gutsol, A. Fridman, Atmospheric pressure plasma of dielectric barrier discharges. *Pure Appl. Chem.* **77**(2), 487–495 (2005)
45. U. Kogelschatz, B. Eliasson, W. Egli, Dielectric-barrier discharges: principle and applications. *J. Phys. IV France*, **7** (1997)
46. J. Cech, P. Stahel, Z. Navratil, The influence of electrode gap width on plasma properties of diffuse coplanar surface barrier discharge in nitrogen. *Eur. Phys. J. D* **54**, 259–264 (2009)
47. C. Anderson, M. Hur, P. Zhang et al., Two-dimensional space-time-resolved emission spectroscopy on atmospheric pressure glows in helium with impurities. *J. Appl. Phys.* **96**(4), (2004)
48. F. Massines, N. Gherardi, N. Naude, Glow and Townsend dielectric barrier discharge in various atmosphere. *Plasma Phys. Control. Fusion* **47**, B577–B588 (2005). doi:[10.1088/0741-3335/47/12B/S42](https://doi.org/10.1088/0741-3335/47/12B/S42)
49. D. Trunec, A. Brablec, J. Buchta, Atmosphericpressure glow discharge in neon. *J. Phys. D: Appl. Phys.* **34**, 1697–1699. (2001). www.iop.org/Journals/jd, PII: S0022-3727(01)21705-7
50. S. Okazaki, M. Kogoma, M. Uehara et al., Appearance of stable glow discharge in air, argon, oxygen and nitrogen at atmosphericpressure using a 50 Hz source. *J. Phys. D Appl. Phys.* **26**, 889–892 (1993)
51. R.B. Tyata, D.P. Subedi, R. Shrestha et al., Generation of uniform atmosphericpressure argon glow plasma by dielectric barrier discharge. *Pramana, J. Phys. Indian Acad. Sci.* **8**(3), 507–517 (2012)
52. D.P. Subedi, R.B. Tyata, A. Khadgi et al., Treatment of water by dielectric barrier discharge. *J. Sci. Technol. Trop.* **5**, 117–123 (2009)
53. S. Foster, C. Mohr, W. Viol, Investigations of an atmospheric pressure plasma jet by optical emission spectroscopy. *Surf. Coat. Technol.* **200**, 827 (2005)
54. J. Tioshifuji, T. Katsumata, H. Takikawa et al., Cold arc-plasma jet under atmosphericpressure for surface modification. *Surf. Coat. Tech.* **171**, 302 (2003)
55. Y. Takemura, Y. Kubota, N. Yamaguchi et al., Development of atmospheric plasma jet with long flame. *Trans. Plasma Sci.* **26**, 1604 (2009)
56. J. Choi, K. Matsuo, H. Yoshida et al., Double-layered atmospheric pressure plasma jet. *Japanese J. Appl. Phys.* **48** (2009)
57. A. Kuwabara, S. Kuroda, H. Kubot, Effects of electrodepositioning on the atmospheric-pressure DBD plasma torch. *Plasma Process. Polym.* **2**, 305–309 (2005). doi:[10.1002/ppap.200400089](https://doi.org/10.1002/ppap.200400089)
58. D.P. Subedi, R.B. Tyata, A. Shrestha et al., An atmospheric pressure non-thermal plasma jet in nitrogen for surface modification of polyethylene. *J. Sci. Technol. Trop.* **6**, 49–52 (2010)
59. Y. Zhang, X.H. Wen, W.H. Yang, *Plasma Sources Sci. Technol.* **16**, 441–447 (2007)

60. X.M. Zhu, W. Cong-Che, Y.K. Pu, Using OES to determine electron temperature and density in low-pressure nitrogen and argon plasmas. *J. Phys. D: Appl. Phys.* **41** (2008)
61. D.P. Subedi, R.B. Tyata, R. Shrestha et al., An experimental study of atmospheric pressure dielectric barrier discharge (DBD) in argon. *AIP Conf. Proc.* **103** (2014)
62. U.M. Joshi, Surface modification of polymers by 50 Hz dielectric barrier discharge produced in air and argon at atmospheric pressure. Ph.D. thesis, Kathmandu University, Nepal, 2013
63. J.H. Kim, Y.H. Choi, Y.S. Hwang, Electron density and temperature measurement method by using emission spectroscopy in atmospheric pressure nonequilibrium nitrogen plasmas. *Phys. Plasmas.* **13** (2006)
64. O.A. Omarov, S.S. El'darov, A.M. Gadzhiev et al., An investigation of the optical characteristics of a pulse discharge in argon at atmospheric pressure in an external magnetic field. *High Temp.* **41**(2), 161–165 (2003)
65. L. Dong, J. Ran, Z. Mao, Direct measurement of electron density in microdischarge at atmospheric pressure by Stark broadening. *Appl. Phys. Lett.* **86**, 161501–161503 (2005)
66. S.J. Kang, V.M. Donnelly, Optical absorption and emission spectroscopy studies of ammonia-containing plasmas. *Plasma Sources Sci. Technol.* **16**, 265–272 (2007). doi:10.1088/0963-0252/16/2/008
67. N. Britun, M. Gaillard, A. Ricard et al., Determination of the vibrational, rotational and electron temperatures in N₂ and Ar–N₂ rf discharge. *J. Phys. D Appl. Phys.* **40**, 1022–1029 (2007). doi:10.1088/0022-3727/40/4/016
68. J. Tynan, V.J. Law, P. Ward et al., Comparison of pilot and industrial scale atmospheric pressure glow discharge systems including a novel electro-acoustic technique for process monitoring. *Plasma Sources Sci. Technol.* **19** (2010)
69. D. Xiao, C. Cheng, J. Shen et al., Electron density measurements of atmospheric-pressure-non-thermal N₂ plasma jet by Stark broadening and irradiance intensity methods. *Phys. Plasmas.* **21** (2014)
70. C.S. Wong, R. Mongkolnavin, *Elements of Plasma Technology* (Springer, Berlin, 2016)
71. N. Balcon, atmospheric pressure radio frequency discharges, diagnostic and numerical modeling. Ph.D. thesis, Australian National University, Australia, 2007
72. D.T. Burns, Early problems in the analysis and the determination of ozone. *Fresenius J. Anal. Chem.* **357**, 178–183 (1997)
73. M.B. Rubin, The history of ozone. *Bull. Hist. Chem.* **26**(1), 1839–1868 (2001)
74. J. Grundmann, S. Muller, R.J. Zahn, Treatment of soot by dielectric barrier discharges and ozone. *Plasma Chem. Plasma Process.* **25**(5), (2005)
75. Z. Buntat, I.R. Smithand, N.A.M. Razali, Ozone generation using atmospheric pressure glow discharge in air. *J. Phys. D: Appl. Phys.* **42** (2009)
76. R. Bhatta, R. Kayastha, D.P. Subedi et al., Treatment of wastewater by ozone produced in dielectric barrier discharge. *J. Chem.* **2015** (2015)
77. R. Shrestha, U.M. Joshi, D.P. Subedi, Experimental study of ozone generation by atmospheric pressure dielectric barrier discharge. *Int. J. Recent Res. Rev.* **VIII**(4), (2015)
78. M. Sira, D. Trunec, P. Stahel et al., Surface modification of polyethylene and polypropylene in atmospheric pressure glow discharge. *J. Phys. D Appl. Phys.* **38**, 621 (2005)
79. S.K. Oiseth, A. Krozer, B. Kasemo et al., Surface modification of spin-coated high-density polyethylene films by argon and oxygen glow discharge plasma treatments. *Appl. Surf. Sci.* **202**, 92–103 (2002)
80. P. Svarnas, N. Spyrou, B. Held, Polystyrene thin films treatment under DC point-to-plane low-pressure discharge in nitrogen for improving wettability. *Eur. Phys. J. Appl. Phys.* **28**, 105–112 (2004)
81. F. Zhi, Q. Yuchang, W. Hui, Surface treatment of polyethylene terephthalate film using atmospheric pressure glow discharge in air. *Plasma Sci. Technol* **6**, 2576 (2004)
82. U. Kogelschatz, Dielectric-barrier discharges: their history, discharge physics, and industrial applications. *Plasma Chem. Plasma Process.* **23** (2003)
83. E.C. Rangel, G.Z. Gadioli, N.C. Cruz, Investigations on the stability of plasma modified silicone surfaces. *Plasmas Polym.* **9**(1), 35–48 (2004)

84. D.P. Subedi, D.K. Madhup, K. Adhikari et al., Low pressure plasma treatment for the enhancement of wettability of polycarbonate. *Indian J. Pure Appl. Phys.* **46**, 540–544 (2008)
85. B. Luepakdeesakoon, C. Saiwan, J.F. Scamehorn, Contact angle of surfactant solutions on precipitated surfactant surfaces. *J. Surfactants Deterg.* **9**(2), 125–136 (2006)
86. H.W. Fox, W.A. Zisman, The spreading of liquids on low energy surfaces. I. polytetrafluoroethylene. *J. Colloid Sci.* **5**, 514–531 (1950)
87. J. Drelich, J.D. Miller, Examination of Neumann's equation-of-state for interfacial tensions. *J. Colloid Interface Sci.* **167**, 217–220 (1994)
88. N.T. Correia, J.J.M. Ramos, B.J.V. Saramago et al., Estimation of the surface tension of a solid: application to a liquid crystalline polymer. *J. Colloid Interface Sci.* **189**, 361–369 (1997)
89. D.Y. Kwok, C.N.C. Lam, A. Li et al., Measuring and interpreting contact angles: a complex issue. *Colloids Surfaces A: Physiochem. Eng. Asp.* **142**, 219–235 (1998)
90. M. Sira, P. Stahel, V. Bursikova et al., Activation of polyethylene and polypropylene in atmospheric pressure glow discharge. *Czech J. Phys.* **54**, 835–839 (2004)
91. R. Mahlberg, H.E.M. Niemi, F. Denes et al., Effect of oxygen and hexamethyldisiloxane plasma on morphology, wettability and adhesion properties of polypropylene and lignocellulosics. *Int. J. Adhes. Adhes.* **18**, 283–297 (1998)
92. S. Coulombe, V. Léveillé, S. Yonson et al., Miniature atmospheric pressure glow discharge torch (APGD-*t*) for local biomedical applications. *Pure Appl. Chem.* **78**(6), 1147–1156 (2006)
93. G. Fridman, M. Peddinghaus, H. Ayan et al., Blood coagulation and living tissue sterilization by floating-electrodedielectric barrier discharge in air. *Plasma Chem. Plasma Process.* **26**, 425–442 (2006)
94. M. Leduc, D. Guay, R.L. Leask et al., Cell permeabilization using a non-thermal plasma. *New J. Phys.* **11** (2009)
95. L. Xue-Chen, J. Peng-Ying, Y. Ning et al., Aspects of the upstream region in a plasma jet with dielectric barrier discharge configurations. *Chin. Phys. B* **21**(4), 1–6 (2012)
96. R. Foest, E. Kindel, A. Ohl et al., RF capillary jet—a tool for localized surface treatment. *Contrib. Plasma Phys.* **47**, 72–77 (2007)